HHS Public Access

Author manuscript

Cell Rep. Author manuscript; available in PMC 2024 September 17.

Published in final edited form as:

Cell Rep. 2020 December 29; 33(13): 108598. doi:10.1016/j.celrep.2020.108598.

Ythdf m^{6}A Readers Function Redundantly during Zebrafish Development

Cassandra Kontur[1,*], **Minsun Jeong**[5], **Daniel Cifuentes**[4], **Antonio J. Giraldez**[1,2,3,6,*]

[1]Department of Genetics, Yale University School of Medicine, New Haven, CT 06510, USA

[2]Yale Stem Cell Center, Yale University School of Medicine, New Haven, CT 06510, USA

[3]Yale Cancer Center, Yale University School of Medicine, New Haven, CT 06510, USA

[4]Department of Biochemistry, Boston University School of Medicine, Boston, MA 02118, USA

[5]Chey Institute for Advanced Studies, Seoul 06141, Republic of Korea

[6]Lead Contact

SUMMARY

During the maternal-to-zygotic transition (MZT), multiple mechanisms precisely control massive decay of maternal mRNAs. N^6-methyladenosine (m^{6}A) is known to regulate mRNA decay, yet how this modification promotes maternal transcript degradation remains unclear. Here, we find that m^{6}A promotes maternal mRNA deadenylation. Yet, genetic loss of m^{6}A readers Ythdf2 and Ythdf3 did not impact global maternal mRNA clearance, zygotic genome activation, or the onset of gastrulation, challenging the view that Ythdf2 alone is critical to developmental timing. We reveal that Ythdf proteins function redundantly during zebrafish oogenesis and development, as double Ythdf2 and Ythdf3 deletion prevented female gonad formation and triple Ythdf mutants were lethal. Finally, we show that the microRNA miR-430 functions additively with methylation to promote degradation of common transcript targets. Together these findings reveal that m^{6}A facilitates maternal mRNA deadenylation and that multiple pathways and readers act in concert to mediate these effects of methylation on RNA stability.

In Brief

Kontur et al. use transcriptomic analysis to reveal that N^6-methylation (m^{6}A) drives mRNA deadenylation of maternally provided mRNAs, whose decay is essential for embryogenesis. Genetic deletion of the Ythdf proteins that serve as m^{6}A effectors reveals that they function redundantly to facilitate both oogenesis and early development.

*Correspondence: cassandra.n.kontur@gmail.com (C.K.), antonio.giraldez@yale.edu (A.J.G.).

AUTHOR CONTRIBUTIONS

C.K., D.C., and A.J.G. conceived of the project. C.K. drove the project and designed the experiments with A.J.G. M.J. performed MZ*dicer* mRNA-sequencing. D.C. generated *ythdf2* and *ythdf3* mutants. C.K. performed the experiments and analysis, and with A.J.G. interpreted the results. A.J.G. supervised the project. C.K. wrote the manuscript with input from A.J.G.

SUPPLEMENTAL INFORMATION

Supplemental Information can be found online at https://doi.org/10.1016/j.celrep.2020.108598.

DECLARATION OF INTERESTS

The authors declare no competing financial interests.

Graphical Abstract

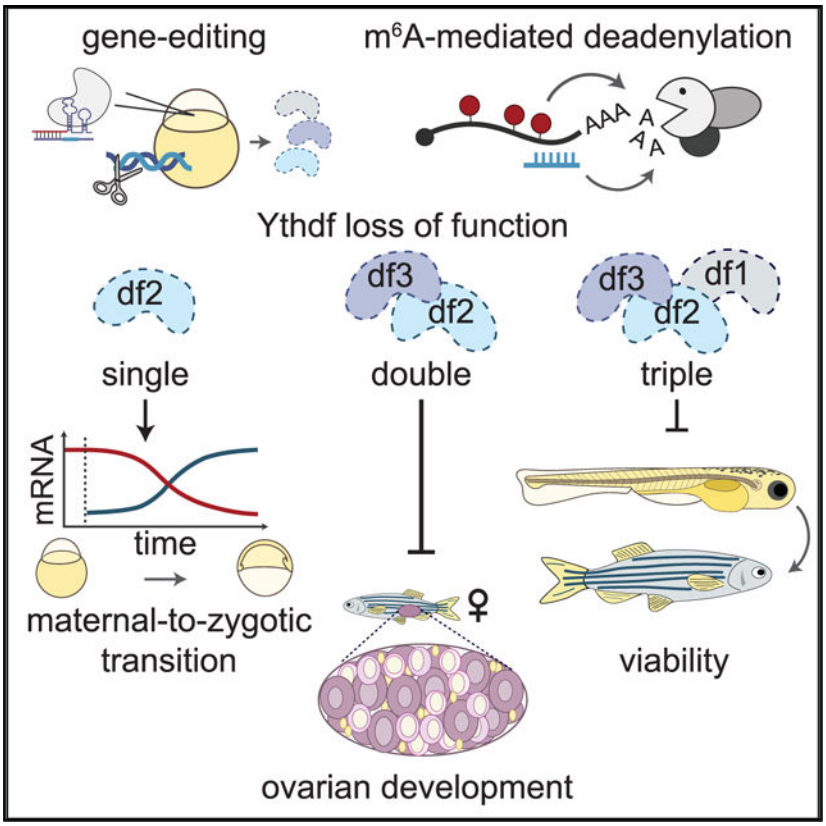

INTRODUCTION

Across metazoans, early embryonic development is directed by maternal gene products, which are required for cellular functions in the initially transcriptionally silent embryo (Laver et al., 2015; Wagner et al., 2004). Developmental control shifts to the zygote during the maternal-to-zygotic transition (MZT), an essential step in animal embryogenesis that is achieved through two interconnected processes: zygotic genome activation (ZGA) and maternal mRNA clearance (Lee et al., 2014; Tadros and Lipshitz, 2009; Vastenhouw et al., 2019). During maternal mRNA clearance, thousands of transcripts are simultaneously degraded (Yartseva and Giraldez, 2015), yet exactly how these mRNAs are eliminated in a precisely timed and coordinated manner remains unresolved.

Several key post-transcriptional mechanisms are known contributors to maternal mRNA clearance, many of which are universal. RNA-binding proteins like Smaug, BRAT, and Pumilio in *Drosophila* (Chen et al., 2014; Gerber et al., 2006; Laver et al., 2015; Newton et al., 2015; Semotok et al., 2005; Tadros et al., 2007; Temme et al., 2010; Weidmann et al., 2014) and EDEN-BP in *Xenopus* (Graindorge et al., 2008; Moraes et al., 2006) bind to mRNA targets and recruit deadenylase machinery to shorten poly(A) tails. MicroRNA-dependent mechanisms, which often promote deadenylation, are also common, with the zygotically transcribed miR-430 destabilizing hundreds of mRNAs in zebrafish (Bazzini

et al., 2012; Giraldez et al., 2006), miR-427 acting in *Xenopus* (Lund et al., 2009), and miR-309 functioning in *Drosophila* (Bushati et al., 2008). Codon optimality also modulates maternal mRNA deadenylation, by sensing the ratio of stabilizing to destabilizing codons, and is conserved to human cells (Bazzini et al., 2016; Mishima and Tomari, 2016; Wu et al., 2019). While these pathways act in concert to destabilize maternal mRNAs, they do not account for all transcript clearance, suggesting that additional mechanisms help govern maternal mRNA decay.

The RNA modification N^6-methyladenosine (m^6A, or RNA methylation) has recently emerged as a new layer of post-transcriptional regulation during developmental transitions (Frye et al., 2018; Roundtree et al., 2017). m^6A is the most prevalent internal mRNA modification and is known to control transcript splicing, turnover, and translation to dictate gene expression changes (Frye et al., 2018; Roundtree et al., 2017; Zaccara et al., 2019). For example, m^6A facilitates degradation of pluripotency promoting mRNAs in mouse embryonic stem cells (Geula et al., 2015) and the m^6A reader YTHDF2 is required to maintain proper transcript levels during murine oogenesis (Ivanova et al., 2017). As more than 30% of zebrafish maternal mRNAs are estimated to contain m^6A, this mark likely also impacts mRNA decay during zebrafish embryogenesis (Zhao et al., 2017). Yet, precisely how RNA methylation contributes to transcript turnover during the MZT remains unclear.

Reader proteins of m^6A, including those of the YTH-domain containing family, are known to recognize and interpret the modification and subsequently induce changes in mRNA fate (Patil et al., 2018; Shi et al., 2019). Initially, the three YTHDF readers were attributed distinct functional roles (Wang et al., 2014, 2015). Yet recent studies have found that the YTHDFs share m^6A binding sites and are simultaneously required for mRNA decay and cellular differentiation, demonstrating that these proteins function redundantly (Lasman et al., 2020; Zaccara and Jaffrey, 2020). All three zebrafish Ythdfs have been identified as maternal mRNA binders through interactome capture experiments (Despic et al., 2017), suggesting that all three paralogs contribute to methylated maternal mRNA decay. Defining the exact roles of the Ythdfs during development is essential to understand precisely how methylation and its readers promote key cellular transitions.

Recently, the reader Ythdf2 was linked to transcriptome turnover during the MZT in zebrafish. In a study by Zhao et al. (2017), Ythdf2 mutants exhibited a developmental delay, which was posited to result from delayed maternal mRNA clearance and ZGA. However, as only the global effect of Ythdf2 on all maternal mRNAs was addressed, how loss of Ythdf2 specifically impacts endogenously methylated mRNAs is yet to be determined. Further, both methylated and unmethylated mRNAs were misregulated in the Ythdf2 mutants, suggesting that either disrupted gene expression resulted indirectly from loss of Ythdf2 or that Ythdf2 exerts a regulatory function independent of m^6A. While work by Zhao et al. (2017) illuminates the role of Ythdf2 during the MZT, it remains unclear how RNA methylation itself guides maternal transcript decay and whether this is dependent on multiple Ythdf factors.

In this study we address the precise contributions of m^6A and the Ythdf readers to the zebrafish MZT. We find that m^6A promoted maternal mRNA deadenylation, but that

this effect was not solely dependent on Ythdf2. We observe that individual Ythdfs were not required for maternal mRNA clearance or developmental timing but that double Ythdf depletion impaired ovary development and triple Ythdf disruption resulted in late-stage larval lethality, suggesting functional redundancy at multiple developmental stages. Together, this work dissects the roles of m^{6}A and its Ythdf readers and reveals how these factors, together with miR-430, contribute to m^{6}A-dependent maternal mRNA clearance.

RESULTS

m^{6}A Modification Promotes Maternal mRNA Deadenylation

While recent work addressed the role of Ythdf2 in the zebrafish MZT (Zhao et al., 2017), we sought to establish the effects of m^{6}A on maternal transcripts directly, by examining how endogenously methylated mRNAs behave during the MZT. To determine whether m^{6}A primarily impacts decay or deadenylation, we compared the stability and poly(A) tails of maternal mRNAs with m^{6}A to a control set of unmodified mRNAs, as detected previously by reported m^{6}A sequencing (Zhao et al., 2017). We observed that methylated transcripts were significantly more deadenylated than unmethylated ones when we analyzed poly(A) tail lengths at 6 hours post fertilization (hpf), as determined from two published datasets in zebrafish embryos, PAL-seq (Subtelny et al., 2014) and TAIL-seq (Chang et al., 2018) (Figure 1A). Differential deadenylation was observed for methylated mRNAs even upon controlling for transcript co-regulation by miR-430 (Figure S1A), which is also known to promote deadenylation (Bazzini et al., 2012; Giraldez et al., 2006). Similarly, we found that the abundance of methylated mRNAs was significantly decreased over time (6 versus 2 hpf) relative to controls in a poly(A)-selected mRNA sequencing time course of zebrafish embryos (Vejnar et al., 2019) (Figure 1B). This effect on transcript abundance remained even after accounting for mRNA expression differences between m^{6}A-modified and unmodified mRNAs (Figure S1B). The differential effect of m^{6}A on transcript levels was less pronounced on mRNA decay than on deadenylation, as changes in total mRNA abundance were more similar for methylated and unmethylated transcripts in rRNA-depleted (ribo0) mRNA sequencing (6 versus 2 hpf; Figures 1C and S1C). We reasoned that differential deadenylation of methylated mRNAs could arise from either stronger deadenylation by 6 hpf or from longer initial poly(A) tails, following the major wave of cytoplasmic polyadenylation that occurs in early embryogenesis (Chang et al., 2018; Subtelny et al., 2014; Ulitsky et al., 2012). To address this, we compared polyadenylation status throughout the MZT, which revealed that methylated mRNAs were more adenylated early at 0 and 2 hpf and had significantly shorter tails at 6 hpf (TAIL-seq and PAL-seq; Figures S1D and S1E). This indicates that methylation is associated with greater initial adenylation, in accordance with previous findings (Aanes et al., 2019), and that it enhances later mRNA deadenylation. Collectively, these analyses suggest that m^{6}A promotes maternal mRNA deadenylation of its target transcripts during the MZT.

To test whether RNA methylation induces transcript deadenylation, we generated an mRNA reporter, made with or without m^{6}A-modified nucleotides, but otherwise identical in sequence (Figure 1D). The reporter was designed without adenosines in the CDS, to test the effects of m^{6}A in the 3′ UTR, as this region is highly linked to regulation of

transcript stability (Charlesworth et al., 2013; Rabani et al., 2017; Vejnar et al., 2019; Voeltz and Steitz, 1998) and is known to harbor m^{6}A modifications (Dominissini et al., 2012; Meyer et al., 2012). To test whether m^{6}A specifically drives tail shortening, we polyadenylated the reporters *in vitro*. Upon injection of reporter mRNA into wild-type embryos, we first observed enhanced deadenylation of the m^{6}A-modified reporter between 0 and 4 hpf relative to the unmodified mRNA. Second, we noted that the m^{6}A reporter exhibited greater degradation by 6 hpf than the unmethylated one (Figure 1E). Thus, m^{6}A both accelerated deadenylation and enhanced subsequent reporter mRNA degradation. This supports our finding that methylation contributes to maternal mRNA clearance by promoting maternal transcript deadenylation and reveals that m^{6}A may also regulate mRNA decay.

m^{6}A-Mediated Maternal mRNA Clearance Is Regulated by the Zygotic Program

Considering the dramatic effect of methylation on maternal mRNA deadenylation, we sought to uncover whether this effect is mediated by maternally or zygotically encoded gene expression programs (Vejnar et al., 2019; Yartseva and Giraldez, 2015). We distinguished between these programs by blocking zygotic transcription with the RNA polymerase II inhibitor, α-amanitin (Kane et al., 1996; Lindell et al., 1970; Vejnar et al., 2019), which revealed that m^{6}A-modified maternal mRNAs were differentially stabilized relative to unmethylated (untreated versus α-amanitin, 6 hpf; Figures 1F and 1G). Next, we tested whether m^{6}A-based degradation depends on zygotic transcription, by injecting our methylated reporter into α-amanitin-treated embryos. When zygotic transcription was blocked, we observed that the m^{6}A-modified reporter no longer decayed by 6 hpf, but unmethylated reporter decay was unaffected (Figure 1H), suggesting that methylated transcripts are more dependent on the zygotic program than are unmethylated. Notably, α-amanitin treatment slowed but did not inhibit methylated reporter deadenylation between 0 and 6 hpf, suggesting that both maternal and zygotic pathways control m^{6}A-mediated tail shortening. Ultimately, these results indicate that a program dependent on zygotic transcription contributes to the degradation of methylation containing mRNAs but that their deadenylation is regulated by both maternal and zygotic programs.

Ythdf2 Is Not Required for Maternal mRNA Clearance and Has Minimal Effects on Methylated mRNA Stability

To identify the pathways controlling m^{6}A-mediated mRNA clearance, we first looked at the role of Ythdf2, which was implicated as a key regulator of decay during the zebrafish MZT (Zhao et al., 2017). To determine whether Ythdf2 is sufficient to drive m^{6}A-mediated maternal mRNA turnover, we performed mRNA sequencing on maternal-zygotic (MZ) mutant embryos with the same *ythdf2* deletion allele as in Zhao et al. (2017) and on related, genetic background-matched wild-type controls (Figure S2A, see discussion). Though Ythdf2 was reportedly required for maternal mRNA clearance, we found no significant differences in abundance for the majority of maternal mRNAs upon loss of Ythdf2 relative to controls, regardless of their methylation status (4 and 6 hpf; Figures 2A, 2B, S2B, and S2C). Indeed, of 13,642 maternally expressed genes, only 18 were found to be differentially expressed at either 4 or 6 hpf (determined by DESeq2; Love et al., 2014; Table S1), and only 2 of these were found to be methylated. Further, only 11 of these 18 transcripts were more abundant at 4 hpf, and only two of these were also more abundant at 6 hpf (Figure

S2D). This discrepancy suggests that the majority of differences in gene expression between MZ*ythdf2* mutants and control embryos may not be due directly from loss of Ythdf2. Thus, although Ythdf2 was proposed as a key regulator of maternal clearance, the fact that maternal transcripts were not majorly stabilized in MZ*ythdf2* mutants demonstrates that Ythdf2 is not obligatory for global maternal mRNA decay.

As maternal transcript decay was largely unaffected in MZ*ythdf2* mutants, we next addressed how Ythdf2 specifically affects methylated mRNAs. When we compared the abundance of m^{6}A-modified and unmodified transcripts, methylated mRNAs were not differentially expressed at 4 hpf, but were marginally more stabilized in the MZ*ythdf2* mutants at 6 hpf, relative to controls (Figures 2C, 2D, S2E, and S2F). While this is consistent with a role for Ythdf2 in methylated mRNA decay, the stabilization of m^{6}A-mRNAs in MZ*ythdf2* mutants is negligible relative to the dramatic stabilization observed in the absence of other key decay regulators (6 hpf, poly(A) mRNA; Figure S2G). For instance, loss of miR-430 through antisense locked nucleic acid (LNA) treatment leads to an average 0.89-fold increase of target transcript abundance, while the fold-change in MZ*ythdf2* mutants was only 0.05 for methylated mRNAs. To further assess the effects of Ythdf2 on m^{6}A-mRNAs, we quantified abundance of several methylated transcripts using qRT-PCR and visualized their expression by *in situ* hybridization. Loss of Ythdf2 did not significantly alter decay of either *zgc:162879* or *mtus1a*, both maternal, m^{6}A-marked transcripts, as levels were comparable to background-matched controls (Figure 2E). Conversely, *mtus1a*, also a miR-430 target, was clearly stabilized in MZ*miR-430* mutants. Together, these data show that loss of Ythdf2 only nominally impedes methylated mRNA degradation and that the contributions of Ythdf2 to m^{6}A-modified maternal transcript clearance are minimal relative to established decay pathways.

Given the extensive effects of m^{6}A on mRNA deadenylation (Figure 1), the minor stabilization of maternal transcripts upon loss of Ythdf2 suggests that it is not the sole regulator of methylated mRNA stability. Indeed, we observed significant stabilization for only 2 of 11 methylated transcripts that were previously defined as Ythdf2 targets (Zhao et al., 2017), as measured by qRT-PCR in MZ*ythdf2* mutants and control embryos (Figure 2F). To further test whether methylated transcripts can be degraded in the absence of Ythdf2, we injected our methylated reporter into MZ*ythdf2* mutants. We found no difference in the adenylation or decay dynamics of the m^{6}A-modified reporter between MZ*ythdf2* and background-matched wild-type embryos (Figure 2G), illustrating that Ythdf2 is dispensable for methylated reporter degradation. Collectively, these experiments reveal that Ythdf2 is not mandatory for clearance of all methylated maternal transcripts, indicating that redundant mechanisms may exist to regulate m^{6}A-mediated decay during the MZT in zebrafish.

Loss of Ythdf2 Does Not Delay Zygotic Genome Activation or Gastrulation

Previous work indicated that loss of Ythdf2 delayed both zygotic genome activation (ZGA) and gastrulation (Zhao et al., 2017), possibly due to slowed maternal clearance. Though our analysis shows that loss of Ythdf2 did not prevent methylated or maternal mRNA clearance, we sought to inspect whether zygotic transcription was disrupted in MZ*ythdf2* mutants. To this end, we compared zygotic gene expression between MZ*ythdf2* mutants

and background-matched wild-type control embryos. Several lines of evidence suggest that Ythdf2 deletion does not hinder the onset of ZGA. First, only 5 of 6,477 zygotic genes were differentially expressed in MZ*ythdf2* mutants relative to controls, and only one of these was downregulated (4 and 6 hpf; Figures 3A, 3B, S2H, and S2I) (DESeq2 analysis; Table S1). Second, when we analyzed the global proportion of intronic reads, used to detect zygotic transcription, we found that intron expression was unchanged in the MZ*ythdf2* mutants relative to wild-type controls, contrasting the sharp intronic read depletion in embryos treated with triptolide, an RNA Pol II inhibitor (Figure 3C). Third, we observed similar RNA levels for several of the earliest expressed zygotic genes including *aplnrb*, *klf17*, and *miR-430*, between MZ*ythdf2* mutants and controls (6 hpf; Figure 3D). These same genes were dramatically downregulated when zygotic transcription was blocked with triptolide. Together, these results illustrate that loss of Ythdf2 does not disrupt zygotic gene expression and thus that Ythdf2 is not essential for the onset nor extent of ZGA.

Given that loss of Ythdf2 did not affect ZGA, we also sought to test whether loss of Ythdf2 disrupts developmental timing during the zebrafish MZT. Consistent with a lack of transcriptomic differences between MZ*ythdf2* mutant and control embryos, we observed no difference in the onset of gastrulation in a live imaging developmental time course (Figure 3E, Video S1). In this time course, we compared MZ*ythdf2* mutants to both related, genetic background-matched wild-type and to unrelated, TU-AB background wild-type embryos (Figure S2A). All embryos were at the 64-cell stage at approximately 2 hpf. However, both MZ*ythdf2* mutants and background-matched controls reached 50% epiboly at approximately ~5.9 hpf, while the TU-AB wild-type reached 50% epiboly about 40 min earlier, at ~5.2 hpf (Figure 3F). This ~40-min delay is consistent with that observed by Zhao et al. (2017), but because this delay was exhibited by both MZ*ythdf2* mutants and background-matched wild-type, it is unlikely to be linked to the *ythdf2* deletion mutation. Indeed, when we injected *ythdf2* mRNA into MZ*ythdf2* mutants, we could not rescue the delay in gastrulation relative to the TU-AB wild-type embryos (Figure S2J). To ensure that Ythdf2 deficiency does not disrupt embryonic development, we generated a second, independent mutant allele of *ythdf2* using CRISPR-Cas9 gene editing (MZ*ythdf2*$^{-223/-223}$) (Figures S2K and S2L). We found no difference in the onset of gastrulation or developmental timing of MZ*ythdf2*$^{-223/-223}$ mutants relative to background-matched controls (Figures 3G and 3H). Thus, loss of Ythdf2 does not disrupt ZGA or the timing of gastrulation, supporting the idea of mechanistic redundancy in methylated maternal mRNA regulation during the MZT.

Deficiency of Ythdf2/Ythdf3 Disrupts Female Gonad Development

Given that Ythdf2 alone did not control timing of the MZT, we sought to establish potentially redundant roles for the Ythdf readers during development. As in humans, zebrafish have three Ythdfs, which exhibit high protein sequence similarity between themselves and with their human orthologs (Figure S3). Further, all three Ythdfs are maternally provided and expressed during the zebrafish MZT (Figures S4A–S4C), reflecting the likelihood of simultaneous activity. We used CRISPR-Cas9 gene editing to individually disrupt *ythdf1*, *ythdf2*, and *ythdf3* (Figures S4D, S4E, S2K, and S2L) but deletion of any one reader did not result in developmental phenotypes (Figures S4G and 3G) nor was it sufficient to stabilize the previously defined m^{6}A-containing mRNAs (Figures S4G and 2F).

Because this suggests that these proteins could function redundantly, we generated a double *ythdf2* and *ythdf3* mutant (Figure S5A), as Ythdf3 is also linked to mRNA decay (Shi et al., 2017). Deletion of both *ythdf2* and *ythdf3* specifically disrupted female development, as no double homozygotes (*ythdf2*$^{-/-}$;*ythdf3*$^{-/-}$) were female, while control siblings (*ythdf2*$^{-/+}$;*ythdf3*$^{-/-}$) were an almost equal ratio of males and females (Figure 4A). This male-only phenotype was also observed in *ythdf1*$^{-/-}$;*ythdf2*$^{-/-}$mutants (Figure S5B) but appears specific to double *ythdf* deletion, as single *ythdf* homozygotes could still become female (Figure S5C). As sex determination and gonad development are interdependent in zebrafish (Santos et al., 2017), we hypothesized that loss of *ythdf2* and *ythdf3* prevented proper establishment of the ovaries. Histological staining of gonads from double *ythdf2*$^{-/-}$;*ythdf3*$^{-/-}$mutants revealed underdeveloped juvenile ovaries at 27 days post fertilization (dpf) relative to sibling controls (Figure 4B). By 34 dpf, all homozygous *ythdf2*$^{-/-}$;*ythdf3*$^{-/-}$mutants had developed testes, the default gonad upon disruption of ovary development (Nagabhushana and Mishra, 2016), whereas controls exhibited both ovaries and testes (Figure 4B). Loss of *ythdf2* and *ythdf3* specifically affected ovaries, as male fish developed healthy testes and were fertile at rates similar to wild-type (Figures S5D and S5E). Together, this phenotype of inhibited female gonad development provides evidence for redundant functions of Ythdf2 and Ythdf3 in the establishment of the ovary prior to the MZT.

Ythdf2 and Ythdf3 together Are Not Obligatory for m^{6}A-Dependent Maternal mRNA Clearance

Though Ythdf2 and Ythdf3 function redundantly to establish the ovary, the extent of overlap in Ythdf reader function during the MZT remains unclear. To test the maternal function of Ythdf2 and Ythdf3, we first had to overcome the defect in ovarian development. To this end, we treated growing double *ythdf2*$^{-/-}$; *ythdf3*$^{-/-}$mutants with 17α-ethynylestradiol (EE2), a synthetic estrogen agonist that promotes ovarian development and subsequently increases the number of female offspring (Örn et al., 2003). Double homozygous females were recovered following EE2 treatment (Figure 4C), enabling study of Ythdf2 and Ythdf3 during methylated RNA decay and embryonic development. MZ*ythdf2;*MZ*ythdf3* mutants appeared to be phenotypically normal relative to EE2-treated background-matched controls, as mutant embryos exhibited normal gastrulation, morphology, and developmental timing (Figure 5A).

To determine whether loss of *ythdf2* and *ythdf3* hinders maternal transcript clearance, we performed poly(A) mRNA-sequencing on MZ*ythdf2;*MZ*ythdf3* mutants from EE2-treated fish. When we compared maternal mRNA expression, we found that very few transcripts were stabilized in MZ*ythdf2*;MZy*thdf3* mutants relative to wild-type controls (236 or 256 of 13,642 maternal mRNAs at 4 or 6 hpf, respectively), of which only 20 were found to be methylated (Figures 5B and S6A). Thus, double Ythdf2 and Ythdf3 deletion did not stabilize most maternal mRNAs, supporting the possibility that other factors also regulate methylated mRNA fate. As loss of Ythdf2 and Ythdf3 did not disrupt maternal clearance, we next tested their role on maternal mRNA deposition and stability, by analyzing maternal transcript levels in the early embryo. Consistent with later time points, abundance was not dramatically altered in MZ*ythdf2;*MZ*ythdf3* mutants at either 0 or 2 hpf (Figures S6B and S6C), as only 130 and 148 of the 13,642 maternal transcripts were stabilized relative to

controls, respectively. Together, this suggests that while Ythdf2 and Ythdf3 are essential to establish the ovary in the zebrafish, they are not compulsory to regulate global maternal transcript levels during the MZT.

To test whether loss of *ythdf2* and *ythdf3* affected decay of methylated mRNAs, we compared changes in maternal transcript abundance between m^{6}A-modified and unmodified mRNAs. As in MZ*ythdf2* embryos, we found that m^{6}A-modified transcripts were slightly stabilized in MZ*ythdf2;*MZ*ythdf3* mutants at 4 and 6 hpf relative to controls (poly(A) and ribo0; Figures S6D–S6F). Yet, as in wild-type embryos, methylated transcripts were still differentially deadenylated in the MZ*ythdf2;*MZ*ythdf3* mutants (0 versus 4 hpf, poly(A); Figure 5C). Further, we did not observe significant stabilization for any of the previously defined m^{6}A-containing targets in MZ*ythdf2;*MZ*ythdf3* mutants relative to background-matched controls, as measured by qRT-PCR (Figure S6G). This suggests that m^{6}A-based recognition and deadenylation of cognate mRNAs was still active in the MZ*ythdf2;*MZ*ythdf3* mutants.

Given that Ythdf2 and Ythdf3 double deletion did not stabilize maternal mRNAs, we generated a triple Ythdf loss-of-function mutant (Figure 5D). Triple *ythdf* disruption was lethal, as triple homozygous larvae could only survive until 9 dpf, likely due to maternally contributed Ythdf proteins (Figure 5E). Triple *ythdf* mutants were never observed in adulthood, and we recovered fewer zebrafish double homozygous for two *ythdf*s and heterozygous for the remaining *ythdf* than expected (Figure 5F). This suggests that the Ythdf proteins act redundantly to ensure zebrafish viability, likely in a dosage-dependent manner, as fewer fish with only one functional *ythdf* copy survived. Unfortunately, the lethality phenotype prohibits analysis of triple Ythdf depletion on methylated mRNA stability and assessment of redundancy during the MZT. Yet, our double and triple *ythdf* mutants demonstrate that dual loss of both Ythdf2 and Ythdf2 was not enough to disrupt preferential deadenylation of methylated mRNAs and reveals that the redundant functions of all three Ythdf readers are required during early development.

miR-430 and m^{6}A Modifications Co-regulate Maternal Transcript Degradation

As loss of *ythdf2* and *ythdf3* did not inhibit methylated mRNA decay, we examined whether a known regulator of maternal clearance, miR-430 (Bazzini et al., 2012; Giraldez et al., 2006), is required to degrade m^{6}A marked transcripts. Notably, we observed that more than a third of methylated maternal mRNAs also contain a miR-430 seed in their 3′ UTR (Figure 6A), consistent with previous reports (Aanes et al., 2019; Zhao et al., 2017), and indicating that these pathways may attenuate stability of shared targets. To disentangle the roles of m^{6}A and miR-430 (Figure 6B), we compared the abundance of transcripts that contained m^{6}A marks, miR-430 seeds, both, or neither during the MZT. mRNAs containing both m^{6}A sites and miR-430 sites were the most degraded, followed sequentially by miR-430 only, methylation-only, and non-target mRNAs (6 versus 2 hpf; Figures 6C and 6D). The effects of m^{6}A and miR-430 were greater in the poly(A) sequencing, as changes in poly(A) mRNA levels likely reflect enhanced deadenylation driven by m^{6}A and miR-430, combined with their milder effects on decay. Further, we found that loss of *miR-430* stabilized only its cognate mRNAs and did not obstruct turnover of m^{6}A-only mRNA, when we

compared wild-type and MZ*dicer* or LNA-treated embryos (Figures 6E and 6F). Together, this suggests that m^{6}A drives mRNA deadenylation independently of miR-430 and that these mechanisms function additively to co-regulate a subset of maternal transcripts for stronger degradation. Indeed, miR-430 contributes greatly to clearance of methylated mRNAs, as the average stabilization of shared miR-430 and m^{6}A targets was approximately 10-fold greater upon loss of miR-430 than loss of either *ythdf2* alone or *ythdf2* and *ythdf3* together (Figure S2G). Thus, the miR-430 pathway acts independently from the mechanism of m^{6}A-mediated mRNA decay but functions combinatorially alongside methylation to co-regulate a subset of highly degraded targets.

DISCUSSION

How multiple post-transcriptional mechanisms are integrated to precisely remove thousands of maternal mRNAs remains an unresolved question. Our study examined how RNA methylation contributes to transcript clearance during the vertebrate MZT and revealed that m^{6}A promotes poly(A) tail shortening of maternal mRNAs. This is consistent with previous findings that m^{6}A promotes deadenylation in cell culture (Du et al., 2016). Indeed, we observed that the effects of m^{6}A were greater on deadenylation than decay for endogenous mRNAs (Figures 1B and 1C), which may reflect the combined effects of poly(A) tail-shortening and mRNA decay driven by m^{6}A when assaying poly(A)-selected mRNA. Further, the rapid deadenylation and enhanced degradation of the methylated reporter (Figure 1E) may reflect its hyper-methylated state, or indicate that m^{6}A-mediated deadenylation enables subsequent and rapid decay. It remains to be determined whether m^{6}A-dependent deadenylation during the MZT is coupled to other m^{6}A-driven decay pathways, such as endoribonucleolytic cleavage (Park et al., 2019) or localization to P-bodies (Ries et al., 2019; Wang et al., 2014). The extent to which m^{6}A-based deadenylation is essential for maternal mRNA clearance is also unknown, as our attempts to remove maternal methylation were frustrated by the larval lethal phenotypes of *mettl3* and *mettl14* (Figure S6H), the core components of methyltransferase complex. Despite this limitation, our work provides mechanistic insight that m^{6}A fosters maternal mRNA deadenylation, establishing it as an important regulator of maternal mRNA clearance. While we find that m^{6}A promotes maternal mRNA deadenylation, we could not establish Ythdf2 as the sole mediator of these effects. Indeed, we show that Ythdf2 is not obligatory for maternal mRNA decay, ZGA, or the onset of gastrulation during the zebrafish MZT, in contrast to previous reports (Zhao et al., 2017). Differences in the observed MZ*ythdf2* phenotype may arise from differences in the genetic background of control embryos (Figure S2A). Indeed, we found that the delay phenotype did not segregate with the *ythdf2* mutation, as it was no longer observed when the genetic background between MZ*ythdf2* mutants and wild-type controls was matched (Figures 3E and 3F). This also accounts for the transcriptomic differences; if mutant embryos are a stage behind developmentally, their gene expression profiles will be consistent with that earlier developmental stage, rather than arising from misregulation of mRNAs due to loss of *ythdf2*. Thus, our data challenge the current view that Ythdf2 is required for proper transcript clearance and ZGA, and indicate instead that Ythdf2 is not obligatory to direct the MZT. Further, we find only a minor role for Ythdf2 in the clearance of methylated transcripts. RNA-sequencing data from both this study and Zhao et al. (2017),

demonstrate that loss of Ythdf2 stabilized few methylated transcripts (Figures S6I and S6J), suggesting that other factors are required for turnover of most m^{6}A targets. Additionally, we do not know what fraction of a given transcript is methylated. Thus, even if Ythdf removal appreciably impacts a small fraction of methylated transcripts, this impact would be masked by the unchanged stability of the larger, unmodified fraction of the same transcript. Yet, the methylated reporter was still rapidly deadenylated and degraded in MZ*ythdf2* mutants (Figure 2G), indicating that loss of Ythdf2 had only minor effects even when the full transcript fraction is methylated. Further, m^{6}A promotes degradation to a similar extent as miR-430 (Figure 6C), but loss of Ythdf2 had a weak effect relative to loss of miR-430 (Figure S2G), suggesting Ythdf2 has a more minor role in clearance of its cognate mRNAs. Thus, while m^{6}A exerts a great effect on maternal mRNA deadenylation, this effect is not majorly controlled by Ythdf2.

Recently, a new model of functional redundancy between the YTHDF proteins has emerged, upending the traditional view that each reader has a distinct regulatory role (Lasman et al., 2020; Zaccara and Jaffrey, 2020). A study from Zaccara and Jaffrey (2020) revealed that all three YTHDF paralogs bind the same m^{6}A sites throughout the transcriptome and highlighted technical and bioinformatic limitations of reports that proposed selective binding. Further, triple YTHDF depletion was required to disrupt methylated mRNA decay in human cells (Zaccara and Jaffrey, 2020), and triple or double YTHDF knockouts exhibited the most severe phenotypes in gametogenesis and viability in mice (Lasman et al., 2020). This is consistent with our findings that individual knockouts did not impede maternal mRNA decay or embryonic development, but that dual loss of Ythdf2 and Ythdf3 impaired oogenesis and triple Ythdf loss led to lethality. Together with these studies, our findings support a mechanism of dosage-dependent functional redundancy of the Ythdf readers. While unique Ythdf functions could arise from exclusive expression of a single paralog in a given cell or tissue (Shi et al., 2019), compartmentalization is unlikely during the zebrafish MZT, as all three Ythdf proteins are simultaneously expressed in the early embryo (Figures S4A–S4C). Ultimately, loss of all three Ythdf readers during the MZT is required to determine whether these factors act redundantly to modulate methylated mRNA fate. Additionally, other proteins have been found to associate with methylated mRNAs (Edupuganti et al., 2017; Huang et al., 2018), expanding the pool of possible m^{6}A regulators. The roles of these proteins and other m^{6}A readers, including Ythdc1 and Ythdc2, must be fully defined to completely elucidate how methylation governs mRNA clearance during key cellular transitions.

Double mutation of *ythdf2* and *ythdf3* resulted in impaired female gonad development, consistent with previous works proposing m^{6}A and its effectors as regulators of gametogenesis. In mice, YTHDF2 was shown to be required for oocyte maturation (Ivanova et al., 2017) and YTHDC1 and YTHDC2, were found to be essential for proper spermatogenesis and oogenesis (Bailey et al., 2017; Hsu et al., 2017; Jain et al., 2018; Kasowitz et al., 2018; Wojtas et al., 2017). It remains unclear exactly how YTHDF readers regulate mRNA stability during oogenesis, as loss of YTHDF2 in mouse oocytes resulted in both transcript up- and downregulation (Ivanova et al., 2017). Regardless of the nature of regulation, the Ythdf paralogs likely function redundantly in the context of gametogenesis, as the male-only phenotype was also observed in double *ythdf1;ythdf2* mutants (Figure

S5B). Future research is required to investigate precisely how overlapping Ythdf function controls mRNA fate to promote vertebrate oogenesis.

Our work also found that RNA methylation functions independently but additively with the miR-430 pathway to target maternal mRNAs for clearance. This sort of combinatorial regulation is thought to serve as a mechanism to ensure that selected transcripts are rapidly and robustly eliminated (Vejnar et al., 2019; Yartseva and Giraldez, 2015). Indeed, we found that mRNAs targeted by both m^6A and miR-430 were the most degraded (Figure 6C). Thus, by combining multiple pathways, different transcripts are conferred different degrees of destabilization, allowing for dynamic regulation in the timing and extent of mRNA decay. Future work is required to determine whether m^6A interacts with other decay programs, such as terminal uridylation, which is known to help degrade maternal transcripts with short poly(A) tails (Chang et al., 2018) during the MZT. Similarly, codon optimality is known to modulate poly(A) length through the translation of optimal and suboptimal codons (Bazzini et al., 2016; Buschauer et al., 2020; Mishima and Tomari, 2016; Presnyak et al., 2015), and m^6A has been found to disrupt tRNA selection and translation elongation (Choi et al., 2016). Whether RNA methylation enhances the effects of codon optimality by contributing to ribosome pausing remains to be determined.

In summary, this study addresses how multiple mechanisms and factors orchestrate maternal mRNA clearance. Among these many mechanisms is m^6A methylation, which contributes to mRNA decay by facilitating maternal transcript deadenylation. We find that individual Ythdf-dependent control of gene expression is not necessary during the MZT, but that these readers contribute redundantly to oocyte development and viability, establishing them as key mediators of developmental transitions.

STAR★METHODS

RESOURCE AVAILABILITY

Lead Contact—Further information and requests for resources and reagents should be directed to and will be fulfilled by the Lead Contact, Antonio J. Giraldez (antonio.giraldez@yale.edu).

Materials Availability—Antibodies, plasmids, fish lines, and other reagents generated in this study are available upon reasonable request to the Lead Contact. Plasmids generated in this study have been deposited to Addgene (see Key Resources Table).

Data and Code Availability—High throughput sequencing data is publicly accessible in the Sequence Read Archive and at https://data.giraldezlab.org. The accession number for all high throughput sequencing data reported in this paper is SRA: SRP297464. To facilitate data download, SRA (SRx) and internal (AGx) IDs are listed in Table S2. All other relevant data are available from lead contact upon reasonable request.

EXPERIMENTAL MODEL AND SUBJECT DETAILS

Zebrafish maintenance and embryo production—*Danio rerio* (zebrafish) embryos were obtained from natural matings of adult fish of mixed wild-type backgrounds (TU-AB

and TLF strains) of mixed ages, ranging from 5–18 months. Wild-type adults were randomly selected from a set of fish previously allocated for use in the weeks embryos were collected. Embryos from multiple wild-type crosses were pooled, unless performing experiments on mutant and background-matched controls, in which case clutches from individual pairs were analyzed separately. Embryos were grown and staged according to published standards (Kimmel et al., 1995) and all zebrafish and embryo experiments were performed at 28°C. For experiments involving mutants and wild-type controls, fish pairs were mated at the same time to generate synchronously growing embryos. Embryo collections of mutants and background-matched controls were then performed at the same time to ensure that all embryos were time-matched for all experiments. Experimental samples were collected at the developmental stages and times specified in the text. Fish lines were maintained in accordance with the International Association for Assessment and Accreditation of Laboratory Animal Care research guidelines, and animal protocols were approved by Yale University Institutional Animal Care and Use Committee (IACUC).

Treatment of juvenile fish with EE2—17 α-ethynylestradiol (EE2) (Sigma-Aldrich, E4876) was diluted with system water to make a 100,000X stock. Approximately 40 fish were raised in a 10-L tank with EE2 solution at a final concentration of 10 ng/L. Fish water was renewed by dripping 40 L of EE2 solution per day. Fish were treated from 22 to 60 days post fertilization and were sexed for mating 30 days later.

METHOD DETAILS

Embryo treatments and injections—All injections into zebrafish embryos were performed on chorionated, one-cell stage embryos with 1 nL volumes, unless otherwise stated. To inhibit RNA Polymerase II, embryos were bathed in 5.8 mM of triptolide (1:1000 dilution of a 5.8 mM stock in DMSO; Sigma-Aldrich, T3652) or injected with 0.2 ng of α-amanitin (Sigma-Aldrich, A2263) re-suspended in nuclease-free water. Triptolide was selected for experiments that necessitated larger numbers of embryos or when injection was inconvenient, as embryos are bathed in the drug. α-amanitin was selected for experiments involving injection, as it provides a more robust inhibition of transcription. Because treatment with transcriptional inhibitors halts development, drug treated embryos were collected when untreated sibling embryos reached the indicated developmental stage.

To generate rescue constructs, zebrafish *ythdf1*, *ythdf2*, and *ythdf3* were PCR amplified from cDNA from 2 hpf embryos using the oligos listed in Table S3. DNA was ligated into a pHA-SP vector containing a 3x-flag sequence using EcoRI and XhoI restriction sites and In-Fusion cloning (Takara, 639642). Final constructs were confirmed by Sanger sequencing. Constructs were linearized with SalI restriction digest and purified using QIAquick PCR purification kit (QIAGEN, 28104). Linearized DNA was used as a template for *in vitro* transcription (IVT) using the mMessage mMachine SP6 Transcription Kit (Invitrogen, AM1340) to generate capped reporter mRNA. Resultant mRNA was DNase treated and purified using the RNeasy RNA extraction kit (QIAGEN, 74104). Zebrafish embryos were injected with 100 pg of mRNA and expression of the flag-tagged protein was confirmed by western blotting.

Microscopy—All imaging was observed using a Zeiss Discovery V12 stereo microscope and images were captured with an AxioCam MRc digital camera (Carl Zeiss). All imaging experiments were performed at a monitored temperature of 28°C and were repeated with at least three biological samples for each condition. For live imaging time course assays, live dechorionated embryos were mounted in 0.25% low melt agarose (AmericanBio, CAS: 9012-36-6) and imaged at least every two minutes. Imaged embryos were staged according to published standards (Kimmel et al., 1995) at multiple time points to assess for potential developmental delay. Developmental rate of mutants versus wild-type was initially assessed by one experimenter and confirmed by other investigators following genotype blinding. All image analysis was performed using ImageJ (Schneider et al., 2012).

Gene editing and maternal-zygotic mutants—CRISPR-Cas9 gene editing in zebrafish was performed as described in Vejnar et al., 2016. Briefly, sgRNAs targeting each gene were designed using the CRISPRscan tool (crisprscan.org) (Moreno-Mateos et al., 2015). Each sgRNA contained a 52-nt oligo containing the T7 promoter (5′-taatacgactcactata-3′), 20-nt of gene specific target sequence, and a constant tail of 15-nt (5′-ttttagagctagaa-3′) used for annealing by a reverse universal oligo (5′-aaaagcaccgactcggtgccacttttcaagttgataacggactagccttattttaacttgctatttctagctctaaaac-3′) to add the invariable 3′ end of the sgRNA. After PCR amplification, products were purified using QIAquick PCR purification kit (QIAGEN, 28104). sgRNAs were synthesized from the purified PCR product by T7 IVT using an AmpliScribe-T7-Flash Transcription kit (Epicenter, ASF3257), reaction at 37°C for 6 h). sgRNAs were DNase-treated, purified by sodium acetate and ethanol precipitation, and checked for RNA integrity by agarose gel electrophoresis.

For gene editing to generate *ythdf2*$^{-223/-223}$ and *ythdf3* mutants, 30 pg of each sgRNA was co-injected with 150 pg of Cas9 (plasmid pT3TS-nCas9n, Addgene #46757, (Jao et al., 2013)) capped mRNA synthesized using mMessage mMachine T3 Transcription kit (Thermo Fisher Scientific, AM1340). For mutagenesis of *ythdf1*, 20 pg of each sgRNA and 150 pg of Cas9 mRNA was co-injected with 20 pg of a single-stranded DNA template (*ythdf1* 5′-gggcagccattgctagcaaaccggccaagcctcagcaactgaaggtgaagagtaagccagggatgcccatgtagtagtagaccaactcgcgtgacacacaggaggtgcctctggaa-3′) to facilitate large deletion and insertion of a stop codon cassette (TAGATAGATAG) by homologous recombination. Mosaic F0 founders were identified by genotyping with oligos corresponding to each target deletion, listed below. Fish were backcrossed twice to wild-type fish before incrossing heterozygous adults to generate homozygous mutants. Homozygous fish were then incrossed to generate maternal-zygotic mutant embryos. Homozygous *ythdf2*$^{-8/-8}$ zebrafish were generated by Zhao et al., 2017 and were obtained from the laboratory of Robert Ho. Double and triple mutants were generated by crossing fish heterozygous for each gene mutation, and then incrossing double or triple heterozygous. These fish were subject to EE2 treatment, to generate both male and female double or triple homozygous. Males and females with double homozygous genotypes were subsequently incrossed to generate maternal-zygotic embryos.

To genotype zebrafish, DNA was extracted from embryos or tissue clipped from the end of the zebrafish tail. Samples were incubated in 100 μL of 100 mM NaOH at 95°C for 20

min and neutralized with 40 μL of 1 M Tris, pH 7.4 (AmericanBio, AB14044). 1 μL of crude DNA extraction was used as a template for PCR using Taq polymerase and indicated genotyping oligos. For the genotyping time course of triple *ythdf* mutants, 48 embryos were removed at random from the pool of offspring every 3 days and subject to genotyping, without being returned to the pool. At 30 dpf, an additional 200 fish were also genotyped.

For experiments comparing MZ mutants to wild-type embryos, wild-type controls were generated from incrossing background-matched wild-type adults that were siblings with homozygous mutants (Figure S2a). This was done to homogenize the genetic background between homozygous MZ mutants and wild-type controls. Background-matched wild-type embryos were used as wild-type controls for all experiments involving MZ mutants, unless otherwise noted. As an additional control, some experiments included embryos generated by crossing unrelated, wild-type fish from TU-AB stock. Oligonucleotides used for sgRNA synthesis and genotyping are listed in Table S3.

Reporter construction and injection—The methylated reporter was generated as follows: DNA fragments for the coding sequence (CDS) and 3′ untranslated region (UTR) were ordered as gBlocks Gene Fragments from IDT. The CDS was designed without adenine in the sequence (with the exception of the ATG start codon, TGA stop codon, and HA tag) to limit incorporation of m^6A to the 3′ UTR during the IVT reaction. The 3′ UTR was designed with 12 copies of the GGACT methylation motif. DNA fragments were PCR amplified for In-Fusion cloning with oligonucleotides listed in Table S3. The pCS2+ vector was linearized with BamHI, and fragments were ligated with the In-Fusion HD enzyme (Takara, 639642). Adenines in the 5′UTR were converted to thymines using site directed mutagenesis with oligos 5′-TTTCTTGCTTCTTGTTCTTTTTGCTGGTTCCATGGCCCGCCTTTGTGCTGC-3′ and 5′-GGAACCAGCAAAAAGAACAAGAAGCAAGAAATCTATAGTGTCACCTAAAT-3′ followed by DpnI digest to remove non-mutated plasmid. Final constructs were confirmed by Sanger sequencing. Plasmids were linearized with XbaI. Capped reporter mRNA was generated by IVT using the HiScribe SP6 RNA Synthesis Kit (New England BioLabs, E2070S) with the addition of 40 mM $m^7G(5′)ppp(5′)G$ RNA cap structure analog (New England BioLabs, S1404S). For methylation containing reporters, 50 mM of N^6-methyladenosine 5′ triphosphate (TriLink, N-1013–5) was added to the IVT in place of adenine. m^6A-IP verified the presence of m^6A modifications in the reporter mRNA. mRNAs were DNase treated following IVT. The poly(A) tail was added after IVT using the Poly(A) tailing kit (Invitrogen, AM1350) according to the manufacturer's instructions. Resultant mRNA was purified using the RNeasy RNA extraction kit (QIAGEN, 74104). Reverse transcription followed by Sanger sequencing of the methylated reporter mRNA confirmed proper incorporation of m^6A only as specified by the plasmid sequence. Zebrafish embryos were injected with 35 pg of either m^6A-modified or unmodified reporter mRNA. Thirty embryos were collected for each condition at different time points during the MZT for RNA extraction and subsequent Northern blot analysis.

RNA isolation—Total RNA was extracted from zebrafish embryos using the TRIzol reagent (Invitrogen, 15596–018) according to the manufacturer's protocol and eluted in

RNase-free water. RNA isolated for qRT-PCR was treated with TURBO DNase (Invitrogen, AM2238) at 37°C for 20 min following RNA extraction and purified using phenol chloroform extraction.

Northern blot analysis—Briefly, 3 μg of total RNA was resuspended in formamide and 2x tracking dye (1mM EDTA, 60 mM triethanolamine, 60 mM tricine, 0.04% bromophenol blue, 2.5% formaldehyde) and heated at 65°C for 10 min to denature the RNA. Samples were separated by electrophoresis using a 1.5% agarose/1.25% formaldehyde gel in 1x Tri/Tri buffer (30 mM triethanolamine, 30 mM tricine). The gel was capillary transferred to a Nytran SPC membrane (Whatman, 10416294). RNA was crosslinked to the membrane with 254 nm UV light at 1200 mJ. Membranes were prehybridized with 5 mL of ExpressHyb hybridization solution (Clontech, 686831) for 1 h at 68°C with constant rotation. RNA species were detected by either cDNA or oligonucleotide probes hybridized at 68°C or 42°C, respectively, overnight with 5 mL of ExpressHyb solution and 5,000,000 cpm of either the reporter or the 18S control radiolabeled probes:

reporter mRNA 5′-
GTCCTTTCTGCTGGTCCTTCCTGTGGGGGTGTCCTGTGTGGGGCCGTGCTTTGGG
CTGCCGTGCTGTCTGCTGGCCCCCTCTGCGCTGGTCCGCTTTGCGGGGGTCGCCT
GTTGGCTGCCCGTCTCTGCGGGGGTCGTCTGTTGGGGGGCCCTCTCTGGGCTGGC
GTTTCCTCTGCTGGTCCGTCCTTGTTCGGCGTTCTCTGTT-3′

Internal 18S maternal rRNA 5′-
CGTTCGTTATCGGAATCAACCAGACAAATCGCTCCACCAACTACGAACGG-3′

Internal 18S somatic rRNA 5′-
CCGTTCTTAGTTGGTGGAGCGATTTGTCTGGTTCATTCCGATAACGAACGAG-3′

cDNA probes were radiolabeled with α-P^{32}-dATP using the Nick Translation Kit (Sigma-Aldrich, 10976776001) according to the manufacturer's protocol. Oligo probes were radiolabeled by T4 PNK end labeling (New England BioLabs, M0201S) with γ-P^{32}-ATP. Radiolabeled probes were purified using ProbeQuant G-50 Micro Columns (GE Healthcare, 28903408) and cDNA probes were heated at 95°C for 5 min prior to hybridization. Membranes probed by cDNA were washed three times with 2x SSC/0.05% SDS for 15 min and twice with 0.1x SSC/0.1% SDS for 20 min at 50°C. Membranes probed with oligos were washed once with 2x SSC/0.05% SDS for 10 min at room temperature and once with 0.1x SSC/0.1% SDS for 2 min at 42°C. Northern blots were quantitated using a phosphorimager (Bio-Rad Personal Molecular Imager). Levels of reporter mRNA were normalized to 18S rRNA controls.

In situ* hybridization—In situ* hybridization was performed as in Thisse and Thisse (2014). To generate antisense RNA *in situ* probes, transcript regions were amplified from zebrafish cDNA using the oligos listed in Table S3. The reverse-orientation oligo contained a T7 promoter overhang for probe synthesis by IVT using T7 polymerase. IVT reactions of 20 μL contained 100 ng of purified PCR product, 2 μL of 10x T7 reaction buffer (New England BioLabs), 1 μL of T7 RNA Polymerase (New England BioLabs, M0251S), 2

µL of 10x DIG RNA labeling mix (Roche, 11 277 073 910), 0.5 µL of RNase inhibitor (RNaseOUT, Invitrogen, 10777019), and nuclease-free water. Probes were purified using the RNeasy RNA extraction kit (QIAGEN, 74104). Each 200 µL hybridization reaction used 20 ng of DIG-labeled RNA probe. Before imaging, embryos were cleared with 2:1 benzyl benzoate:benzyl alcohol solution. For each condition, at least 20 embryos were analyzed and all displayed comparable levels of staining following equal stain time. Imaging was performed using a Zeiss Discovery V12 stereo microscope. Maternal-zygotic mutant embryos of *miR-430* were collected from an incross of homozygous *miR-430* deletion fish from Liu et al. (2013). Wild-type control embryos used for *in situ* experiments were background-matched wild-type relatives of MZ*ythdf2* embryos.

qRT-PCR measure of RNA abundance—Total RNA was extracted from 20 embryos per experimental condition and DNase treated. cDNA was synthesized from 1 µg of total RNA using reverse transcription with random hexamers and the Superscript III reverse transcriptase kit (Invitrogen, 18080093). cDNA was diluted 1:20 and 10 µL reactions for PCR reactions were prepared with 5 µL of Power SYBR Green PCR Master Mix (Applied Biosystems, 4368706), 4.5 µL of 1:100 diluted cDNA, and 0.5 µL of 10 mM forward and reverse primer mix. At least two biological and two technical replicates were performed for each sample. Relative expression was measured with ViiA 7 software v1.2.2 using the ΔΔCT method, with *dcun15d* as a reference control. Oligonucleotides used for qRT-PCR are listed in Table S3.

Immunoprecipitation and western blotting—Fifty embryos were collected, flash frozen in liquid nitrogen, and resuspended in 150 µL lysis buffer (150 µM NaCl, 25 mM Tris-HCl, 1 mM EDTA, 1% Igepal CA-630, 0.1% SDS) with 1X protease inhibitor cocktail (Roche, 11873580001). Lysates were incubated at 4°C for 10 min, followed by centrifugation at 14000 rpm for 15 min at 4°C. Supernatants were added to antibody-coupled Protein A Dynabeads (Invitrogen, 10008D) (10 µL of beads and 1.5 µg of antibody, coupled according to manufacturer's protocol). Lysates and antibodies were incubated at 4°C for at least two h, with rotation. Prior to washes, 20 µL of supernatant was removed for input control. Beads were then washed three times in lysis buffer and resuspended in sample buffer (7.5 µL of 4x NuPAGE LDS Sample Buffer (Invitrogen, NP0321PK2), 3 µL of 1 M DTT (Sigma-Aldrich, 43816), 19.5 µL of nuclease-free water). Samples were heated at 70°C for 10 min and separated on a 1.0 mm 4%–12% Bis-Tris NuPAGE mini protein gel (Invitrogen) at 180 V for 50 min and wet transferred onto a nitrocellulose membrane (GE LifeSciences) at 20 V for 4 h. Membranes were blocked in 5% milk, 1% Tween-20 in PBS for 1 h and then incubated overnight at 4°C with constant rotation in anti-Ythdf1, Ythdf2, or Ythdf3 antibody diluted 1:1000 or in anti-Actin diluted 1:5000 in block buffer. Secondary antibody Goat Anti-rabbit IgG antibody (H+L) HRP conjugate (Millipore, AP307P) was diluted 1:10,000 in block buffer and the membrane was incubated for one h at room temperature. Membranes were washed three times for 5–10 min after each antibody incubation. Membranes were developed by chemiluminescent detection using ECL western blotting substrate (Thermo Fisher, 34095) and imaged by and X-ray film (Denville Scientific, E3012). Actin was used as a loading control for input for immunoprecipitated samples.

Antibodies against Ythdf1, Ythdf2, and Ythdf3 were custom generated by YenZyme by raising antibodies in rabbit against amino acid sequences as follows: CKNLEPAPIQNRSRLDQERQ for Ythdf1, PQQTSLPTNGQPPNQSSPQ for Ythdf2, and RNRGTMFNQNSGMDN for Ythdf3 (amino acid sequences are listed from N to C terminus). Western blot analysis detected a ~65 kDa band in zebrafish lysates when probed with antibody but not with pre-immune serum. The antibody was specific for each Ythdf, as it did not recognize flag-tagged versions of the other two Ythdf proteins.

Histology—For juvenile fish aged either 27- or 34-days post fertilization, heads and tails were removed and the middle body section containing the gonads were fixed in Bouin's solution (Sigma-Aldrich, HT10132) overnight at 4°C. Fixed tissues were embedded in paraffin and sectioned at 10 μm. Hematoxylin and Eosin (H&E) staining was performed on the sections according to standard protocols. Slides were mounted in Omnimount (National Diagnostics, 17997–01) and imaged using a Zeiss Axio Imager M1 and an AxioCam MRc digital camera (Carl Zeiss).

RNA-sequencing library preparation—For RNA-sequencing in *ythdf* mutants, 20 embryos per condition were collected at indicated developmental time points and snap frozen in liquid nitrogen. Embryo collections for mutants and background-matched wild-type were performed at the same time (time-matched), with synchronously developing embryos. Embryos collected across experimental time points came from a single fish couple for each genotype, but different couples were used for each biological replicate. Biological replicates for MZ*ythdf2* mRNA sequencing (named "MZythdf2 vs bkgd-match WT mRNA pA & R0, rep1" and "MZythdf2 vs bkgd-match WT mRNA pA & R0, rep2") were from two independent experiments, with embryo samples collected on different days from different *ythdf2*$^{-/-}$ mutant couples. In the first experimental replicate of MZ*ythdf2* mutant mRNA sequencing only, background-matched controls were from an incross of *ythdf2*$^{+/-}$ fish (meaning embryos had maternally contributed Ythdf2), because no background-matched wild-type fish laid clutches of time-matched embryos on the day of the experiment. For mRNA sequencing of MZ*ythdf2*;MZ*ythdf3*, wild-type controls were unrelated TU-AB wild-type embryos that had not been EE2-treated, because no background-matched wild-type fish laid embryo clutches on the day of the experiment. Background-matched embryos from an incross of EE2-treated fish with the genotype *ythdf2*$^{-/+}$ and *ythdf3*$^{-/-}$ were included as an additional control for this assay. RNA sequencing samples of MZ*ythdf2*;MZ*ythdf3* at 6 hpf were collected at a later date than those from 0, 2, and 4 hpf, and thus no comparisons between 6 hpf and other time points were made. For normalization, *S.cerevisiae* yeast total RNA was spiked into TRIzol (Invitrogen, 15596–018) prior to RNA extraction. Total RNA was then subjected to either poly(A)-selection by oligo(dT) beads or to ribosomal RNA-depletion with Epicenter Ribo-Zero Gold, according to manufacturer's instructions. Strand-specific TruSeq Illumina RNA-sequencing libraries were then constructed, and samples were multiplexed and sequenced on Illumina HiSeq 2500 machines to generate 76-nucleotide single-end reads. Library preparation and mRNA sequencing was performed by the Yale Center for Genome Analysis.

RNA-sequencing analysis—The zebrafish mRNA sequencing embryonic development time course datasets, including treatments of α-amanitin or tiny locked nucleic acid (LNA) complementary to miR-430 were from previously published SRA: SRP189512 (Vejnar et al., 2019), SRA: SRP149556 (Beaudoin et al., 2018), and SRA: SRP072296 (Bazzini et al., 2016) datasets. SRA and internal laboratory run IDs for each sample are described in Vejnar et al. (2019) (Table S2). Updated gene counts, datasets, and genome browser tracks are available at https://data.giraldezlab.org, and RNA expression data used for analysis here was taken directly from these provided tables. MZ*dicer* fish were obtained from Giraldez et al., 2006. Re-analysis of published MZ*ythdf2* RNA-sequencing data was performed on dataset from Zhao et al., 2017, from GEO accession number GSE79213. For all high throughput sequencing experiments, LabxDB was used to store, manage, and integrate data into the bioinformatics pipeline (Vejnar and Giraldez, 2020).

Mapping reads—Raw reads were mapped using STAR (Dobin et al., 2013) version 2.7.1a to the zebrafish GRCz11 reference genome. Reads in datasets containing yeast spike-in were also mapped to yeast R64-1-1 genome. The following non-default parameters were used in mapping:–*alignEndsType*, *Local*,–*outFilterMultimapNmax 100*,–*seedSearchStartLmax 30*, and –*sjdbScore 2*. Genomic sequence indices for STAR were built including exon-junction coordinates from Ensembl v92 (Aken et al., 2017). Gene annotations were created by concatenating all Ensembl transcript isoforms together. To calculate read counts per gene, all reads that mapped uniquely to the genome and overlapped at least ten nucleotides of the gene annotation were summed. Because the *miR-430* locus is internally repetitive, genome tracks for *miR-430* were generated by allowing up to 900 alignments per read. To calculate per gene RPKMs, the total number of RNA reads mapped to each gene were summed and normalized by gene length and the total numbers of reads mapped to the zebrafish transcriptome per million. Though RNA-sequencing datasets included yeast spike-in, counts were normalized relative to zebrafish reads only, to allow for comparisons between datasets that did not include yeast spike-ins. Summary of read mapping is presented in Table S2.

Differential gene expression analysis—To identify significantly differentially expressed genes between background-matched wild-type controls and MZ*ythdf2* mutants, read counts were compared using the R package DESeq2 (Love et al., 2014). Genes were excluded from the analysis if the gene count was below one for both replicates in either condition. To get DE genes, counts for all Ensembl genes were input to the *results* function with the options *pAdjustMethod = 'fdr'* and *independentFiltering = FALSE*. *P*-values reported from DESeq2 are adjusted *P*-values corrected for multiple testing.

Determination of maternal and zygotic genes—Maternal, maternal-zygotic, and zygotic genes were previously defined in Lee et al. (2013). Expression of each gene's exons and introns was used to classify them as maternally or zygotically expressed genes. For analyses here, thresholds were applied to categories in the table provided in Table S1 from Lee et al. (2013). Strictly maternal genes were those labeled maternal (Maternal_contr = M) and with no transcription at 4 hpf in wild-type embryos (WT4_txed = 0). Maternal and maternal-zygotic included all genes labeled maternal (Maternal_contr = M or m). Zygotic genes included all genes labeled zygotic (Maternal_contr = Z). For analyses directly

comparing maternal mRNA abundance between m^{6}A-modified and unmodified mRNAs, only strictly maternal transcripts were included. For analyses analyzing global abundance of maternal mRNAs, both exclusively maternally expressed and maternal-zygotic mRNAs were included.

Methylated and unmethylated gene definition—Datasets for m^{6}A-methylation in zebrafish (Zhao et al., 2017) are available from GEO accession number GSE79213. Genes found to have transcript methylation were defined previously from Zhao et al., 2017, and were taken directly from the provided table of processed data (GSE79213_processed_data_FPKM.xlsx). Ensembl mapping was used to convert ZFIN gene names provided in the table to Ensembl gene and transcript IDs. If a gene had multiple isoforms, the longest transcript isoform was selected for that gene. Maternal m^{6}A-modified transcripts used for analysis here included those that were found to contain m^{6}A-modification in both the m^{6}A-seq and m^{6}A-CLIP-seq from Zhao et al., 2017 at either 0 hpf or 2 hpf.

Poly(A) tail length analysis—Datasets for poly(A) tail length were downloaded from public repositories. PAL-sequencing (Subtelny et al., 2014) was downloaded from GEO accession number GSE52809 and TAIL-sequencing data (Chang et al., 2018) was downloaded from Zenodo https://doi.org/10.5281/zenodo.2640028. For each dataset, the average poly(A) tail length was calculated by averaging counts for the poly(A) tail reads for each gene at each time point. The same sets of methylated and non-methylated transcripts were used to analyze each poly(A) tail dataset.

QUANTIFICATION AND STATISTICAL ANALYSIS

All analyses were performed with custom scripts written in Python 3. For all box and whisker plots, including those presented inside violin plots, boxes extend from the 25th to 75th percentiles, with the center line representing the median value, whiskers representing 1.5x the inter-quartile range, and diamonds indicating outliers. For violin plots without internal box and whisker plot, solid lines represent the median and dashed lines indicated the 25th and 75th percentiles. Bar plots present mean values with standard deviation as the error bars. For expression-matched analysis, methylated mRNAs were divided into quintiles with similar numbers of transcripts in each to determine RPKM cut offs. The unmodified transcripts were then binned using these same cut offs, and average $\log_2$ RPKM fold changes were calculated for each condition in each quintile. miR-430 targets were defined as all maternal transcripts with the miR-430 seed sequence in their 3′ UTR. For the venn diagram, stabilized MZ*ythdf2* transcripts included all maternal transcripts with fold-change > 0.5 ($\log_2$ RPKM), regardless of whether they were determined to be significantly differentially expressed by DESeq analysis. To calculate proportion of intronic reads, the total counts of uniquely mapped intronic reads was divided by the total read count for the respective sample from ribo0 mRNA-sequencing. Sample sizes (n), statistical test outcomes, and significance levels are indicated in figures and figure legends. For comparisons between m^{6}A modified and unmodified mRNAs, statistical significance was computed using the Mann-Whitney U test. For comparisons of a single gene's expression between experimental conditions, the two-sided Student's t test for paired samples was used to determine statistical

significance. Protein sequence alignment was generated using SnapGene® software (GSL Biotech, available at snapgene.com), with Clustal Omega alignment, made relative to the consensus sequence with a consensus threshold of > 50%. Phylogenetic tree was generated from the protein sequence alignment described above using Clustal W2 and neighbor-joining clustering.

Supplementary Material

Refer to Web version on PubMed Central for supplementary material.

ACKNOWLEDGMENTS

We thank Karen Bishop, Nitya Khatri, Sarah Dube, Hiba Codore, Valeria Schmidt, and Timothy Gerson for technical help. We thank Charles Vejnar for assistance in data analysis, Jean-Denis Beaudoin for experimental guidance, and Liyun Miao for help with histology. We thank all Giraldez lab members for intellectual and technical support and suggestions, and for critical reading of the manuscript. We thank K. Bilguvar, S. Mane, and C. Castaldi for sequencing support. We thank Chuan He and Robert Ho for providing *ythdf2* mutant zebrafish and Hyeshik Chang for help processing TAIL-seq data. We thank Samie Jaffrey, Kate Meyer, and Bastian Linder for assistance with miCLIP-seq. The Giraldez lab is supported by the NIH grant R35 GM122580 04, the Howard Hughes Medical Institute Faculty Scholar program, and the Fergus F. Wallace endowment to A.J.G. D.C. was supported by the NIH K99 grant HD071968.

REFERENCES

Aanes H, Engelsen D, Manaf A, Alemu EA, Vagbo CB, Martin L, Lerdrup M, Hansen K, Mathavan S, Winata C, et al. (2019). N6-methyladenosine dynamics during early vertebrate embryogenesis. bioRxiv. 10.1101/528422.

Aken BL, Achuthan P, Akanni W, Amode MR, Bernsdorff F, Bhai J, Billis K, Carvalho-Silva D, Cummins C, Clapham P, et al. (2017). Ensembl 2017. Nucleic Acids Res. 45 (D1), D635–D642. [PubMed: 27899575]

Bailey AS, Batista PJ, Gold RS, Chen YG, de Rooij DG, Chang HY, and Fuller MT (2017). The conserved RNA helicase YTHDC2 regulates the transition from proliferation to differentiation in the germline. eLife 6, 6.

Bazzini AA, Lee MT, and Giraldez AJ (2012). Ribosome profiling shows that miR-430 reduces translation before causing mRNA decay in zebrafish. Science 336, 233–237. [PubMed: 22422859]

Bazzini AA, Del Viso F, Moreno-Mateos MA, Johnstone TG, Vejnar CE, Qin Y, Yao J, Khokha MK, and Giraldez AJ (2016). Codon identity regulates mRNA stability and translation efficiency during the maternal-to-zygotic transition. EMBO J. 35, 2087–2103. [PubMed: 27436874]

Beaudoin JD, Novoa EM, Vejnar CE, Yartseva V, Takacs CM, Kellis M, and Giraldez AJ (2018). Analyses of mRNA structure dynamics identify embryonic gene regulatory programs. Nat. Struct. Mol. Biol 25, 677–686. [PubMed: 30061596]

Buschauer R, Matsuo Y, Sugiyama T, Chen YH, Alhusaini N, Sweet T, Ikeuchi K, Cheng J, Matsuki Y, Nobuta R, et al. (2020). The Ccr4-Not complex monitors the translating ribosome for codon optimality. Science 368, 368. [PubMed: 32327586]

Bushati N, Stark A, Brennecke J, and Cohen SM (2008). Temporal reciprocity of miRNAs and their targets during the maternal-to-zygotic transition in Drosophila. Curr. Biol 18, 501–506. [PubMed: 18394895]

Chang H, Yeo J, Kim JG, Kim H, Lim J, Lee M, Kim HH, Ohk J, Jeon HY, Lee H, et al. (2018). Terminal Uridylyltransferases Execute Programmed Clearance of Maternal Transcriptome in Vertebrate Embryos. Mol. Cell 70, 72–82.e7. [PubMed: 29625039]

Charlesworth A, Meijer HA, and de Moor CH (2013). Specificity factors in cytoplasmic polyadenylation. Wiley Interdiscip. Rev. RNA 4, 437–461. [PubMed: 23776146]

Chen L, Dumelie JG, Li X, Cheng MHK, Yang Z, Laver JD, Siddiqui NU, Westwood JT, Morris Q, Lipshitz HD, and Smibert CA (2014). Global regulation of mRNA translation and stability in the

early Drosophila embryo by the Smaug RNA-binding protein. Genome Biol. 15, R4. [PubMed: 24393533]

Choi J, Ieong KW, Demirci H, Chen J, Petrov A, Prabhakar A, O'Leary SE, Dominissini D, Rechavi G, Soltis SM, et al. (2016). N(6)-methyladenosine in mRNA disrupts tRNA selection and translation-elongation dynamics. Nat. Struct. Mol. Biol 23, 110–115. [PubMed: 26751643]

Despic V, Dejung M, Gu M, Krishnan J, Zhang J, Herzel L, Straube K, Gerstein MB, Butter F, and Neugebauer KM (2017). Dynamic RNA-protein interactions underlie the zebrafish maternal-to-zygotic transition. Genome Res. 27, 1184–1194. [PubMed: 28381614]

Dobin A, Davis CA, Schlesinger F, Drenkow J, Zaleski C, Jha S, Batut P, Chaisson M, and Gingeras TR (2013). STAR: ultrafast universal RNA-seq aligner. Bioinformatics 29, 15–21. [PubMed: 23104886]

Dominissini D, Moshitch-Moshkovitz S, Schwartz S, Salmon-Divon M, Ungar L, Osenberg S, Cesarkas K, Jacob-Hirsch J, Amariglio N, Kupiec M, et al. (2012). Topology of the human and mouse m6A RNA methylomes revealed by m6A-seq. Nature 485, 201–206. [PubMed: 22575960]

Du H, Zhao Y, He J, Zhang Y, Xi H, Liu M, Ma J, and Wu L. (2016). YTHDF2 destabilizes m(6)A-containing RNA through direct recruitment of the CCR4-NOT deadenylase complex. Nat. Commun 7, 12626. [PubMed: 27558897]

Edupuganti RR, Geiger S, Lindeboom RGH, Shi H, Hsu PJ, Lu Z, Wang SY, Baltissen MPA, Jansen PWTC, Rossa M, et al. (2017). N6-methyladenosine (m6A) recruits and repels proteins to regulate mRNA homeostasis. Nat. Struct. Mol. Biol 24, 870–878. [PubMed: 28869609]

Frye M, Harada BT, Behm M, and He C. (2018). RNA modifications modulate gene expression during development. Science 361, 1346–1349. [PubMed: 30262497]

Gerber AP, Luschnig S, Krasnow MA, Brown PO, and Herschlag D. (2006). Genome-wide identification of mRNAs associated with the translational regulator PUMILIO in Drosophila melanogaster. Proc. Natl. Acad. Sci. USA 103, 4487–4492. [PubMed: 16537387]

Geula S, Moshitch-Moshkovitz S, Dominissini D, Mansour AAF, Kol N, Salmon-Divon M, Hershkovitz V, Peer E, Mor N, Manor YS, et al. (2015). Stem cells. m6A mRNA methylation facilitates resolution of naïve pluripotency toward differentiation. Science 347, 1002–1006. [PubMed: 25569111]

Giraldez AJ, Mishima Y, Rihel J, Grocock RJ, Van Dongen S, Inoue K, Enright AJ, and Schier AF (2006). Zebrafish MiR-430 promotes deadenylation and clearance of maternal mRNAs. Science 312, 75–79. [PubMed: 16484454]

Graindorge A, Le Tonquè ze O, Thuret R, Pollet N, Osborne HB, and Audic Y. (2008). Identification of CUG-BP1/EDEN-BP target mRNAs in Xenopus tropicalis. Nucleic Acids Res. 36, 1861–1870. [PubMed: 18267972]

Hsu PJ, Zhu Y, Ma H, Guo Y, Shi X, Liu Y, Qi M, Lu Z, Shi H, Wang J, et al. (2017). Ythdc2 is an N6-methyladenosine binding protein that regulates mammalian spermatogenesis. Cell Res. 27, 1115–1127. [PubMed: 28809393]

Huang H, Weng H, Sun W, Qin X, Shi H, Wu H, Zhao BS, Mesquita A, Liu C, Yuan CL, et al. (2018). Recognition of RNA N6-methyladenosine by IGF2BP proteins enhances mRNA stability and translation. Nat. Cell Biol 20, 285–295. [PubMed: 29476152]

Ivanova I, Much C, Di Giacomo M, Azzi C, Morgan M, Moreira PN, Monahan J, Carrieri C, Enright AJ, and O'Carroll D. (2017). The RNA m6A Reader YTHDF2 Is Essential for the Post-transcriptional Regulation of the Maternal Transcriptome and Oocyte Competence. Mol. Cell 67, 1059–1067.e4. [PubMed: 28867294]

Jain D, Puno MR, Meydan C, Lailler N, Mason CE, Lima CD, Anderson KV, and Keeney S. (2018). ketu mutant mice uncover an essential meiotic function for the ancient RNA helicase YTHDC2. eLife 7, 7.

Jao LE, Wente SR, and Chen W. (2013). Efficient multiplex biallelic zebrafish genome editing using a CRISPR nuclease system. Proc. Natl. Acad. Sci. USA 110, 13904–13909. [PubMed: 23918387]

Kane DA, Hammerschmidt M, Mullins MC, Maischein HM, Brand M, van Eeden FJ, Furutani-Seiki M, Granato M, Haffter P, Heisenberg CP, et al. (1996). The zebrafish epiboly mutants. Development 123, 47–55. [PubMed: 9007228]

Kasowitz SD, Ma J, Anderson SJ, Leu NA, Xu Y, Gregory BD, Schultz RM, and Wang PJ (2018). Nuclear m6A reader YTHDC1 regulates alternative polyadenylation and splicing during mouse oocyte development. PLoS Genet. 14, e1007412.

Kimmel CB, Ballard WW, Kimmel SR, Ullmann B, and Schilling TF (1995). Stages of embryonic development of the zebrafish. Dev. Dyn 203, 253–310. [PubMed: 8589427]

Lasman L, Krupalnik V, Viukov S, Mor N, Aguilera-Castrejon A, Schneir D, Bayerl J, Mizrahi O, Peles S, Tawil S, et al. (2020). Context-dependent functional compensation between Ythdf m6A reader proteins. Genes Dev. 34, 1373–1391. [PubMed: 32943573]

Laver JD, Li X, Ray D, Cook KB, Hahn NA, Nabeel-Shah S, Kekis M, Luo H, Marsolais AJ, Fung KYY, et al. (2015). Brain tumor is a sequence-specific RNA-binding protein that directs maternal mRNA clearance during the Drosophila maternal-to-zygotic transition. Genome Biol. 16, 94. [PubMed: 25962635]

Lee MT, Bonneau AR, Takacs CM, Bazzini AA, DiVito KR, Fleming ES, and Giraldez AJ (2013). Nanog, Pou5f1 and SoxB1 activate zygotic gene expression during the maternal-to-zygotic transition. Nature 503, 360–364. [PubMed: 24056933]

Lee MT, Bonneau AR, and Giraldez AJ (2014). Zygotic genome activation during the maternal-to-zygotic transition. Annu. Rev. Cell Dev. Biol 30, 581–613. [PubMed: 25150012]

Lindell TJ, Weinberg F, Morris PW, Roeder RG, and Rutter WJ (1970). Specific inhibition of nuclear RNA polymerase II by α-amanitin. Science 170, 447–449. [PubMed: 4918258]

Liu Y, Luo D, Zhao H, Zhu Z, Hu W, and Cheng CHK (2013). Inheritable and precise large genomic deletions of non-coding RNA genes in zebrafish using TALENs. PLoS ONE 8, e76387.

Love MI, Huber W, and Anders S. (2014). Moderated estimation of fold change and dispersion for RNA-seq data with DESeq2. Genome Biol. 15, 550. [PubMed: 25516281]

Lund E, Liu M, Hartley RS, Sheets MD, and Dahlberg JE (2009). Deadenylation of maternal mRNAs mediated by miR-427 in Xenopus laevis embryos. RNA 15, 2351–2363. [PubMed: 19854872]

Meyer KD, Saletore Y, Zumbo P, Elemento O, Mason CE, and Jaffrey SR (2012). Comprehensive analysis of mRNA methylation reveals enrichment in 3¿ UTRs and near stop codons. Cell 149, 1635–1646. [PubMed: 22608085]

Mishima Y, and Tomari Y. (2016). Codon Usage and 3¿ UTR Length Determine Maternal mRNA Stability in Zebrafish. Mol. Cell 61, 874–885. [PubMed: 26990990]

Moraes KCM, Wilusz CJ, and Wilusz J. (2006). CUG-BP binds to RNA substrates and recruits PARN deadenylase. RNA 12, 1084–1091. [PubMed: 16601207]

Moreno-Mateos MA, Vejnar CE, Beaudoin JD, Fernandez JP, Mis EK, Khokha MK, and Giraldez AJ (2015). CRISPRscan: designing highly efficient sgRNAs for CRISPR-Cas9 targeting in vivo. Nat. Methods 12, 982–988. [PubMed: 26322839]

Nagabhushana A, and Mishra RK (2016). Finding clues to the riddle of sex determination in zebrafish. J. Biosci 41, 145–155. [PubMed: 26949096]

Newton FG, Harris RE, Sutcliffe C, and Ashe HL (2015). Coordinate post-transcriptional repression of Dpp-dependent transcription factors attenuates signal range during development. Development 142, 3362–3373. [PubMed: 26293305]

Örn S, Holbech H, Madsen TH, Norrgren L, and Petersen GI (2003). Gonad development and vitellogenin production in zebrafish (Danio rerio) exposed to ethinylestradiol and methyltestosterone. Aquat. Toxicol 65, 397–411. [PubMed: 14568354]

Park OH, Ha H, Lee Y, Boo SH, Kwon DH, Song HK, and Kim YK (2019). Endoribonucleolytic Cleavage of m6A-Containing RNAs by RNase P/MRP Complex. Mol. Cell 74, 494–507.e8. [PubMed: 30930054]

Patil DP, Pickering BF, and Jaffrey SR (2018). Reading m6A in the Transcriptome: m6A-Binding Proteins. Trends Cell Biol. 28, 113–127. [PubMed: 29103884]

Presnyak V, Alhusaini N, Chen YH, Martin S, Morris N, Kline N, Olson S, Weinberg D, Baker KE, Graveley BR, and Coller J. (2015). Codon optimality is a major determinant of mRNA stability. Cell 160, 1111–1124. [PubMed: 25768907]

Rabani M, Pieper L, Chew GL, and Schier AF (2017). A Massively Parallel Reporter Assay of 3¿ UTR Sequences Identifies In Vivo Rules for mRNA Degradation. Mol. Cell 68, 1083–1094.e5. [PubMed: 29225039]

Ries RJ, Zaccara S, Klein P, Olarerin-George A, Namkoong S, Pickering BF, Patil DP, Kwak H, Lee JH, and Jaffrey SR (2019). m6A enhances the phase separation potential of mRNA. Nature 571, 424–428. [PubMed: 31292544]

Roundtree IA, Evans ME, Pan T, and He C. (2017). Dynamic RNA Modifications in Gene Expression Regulation. Cell 169, 1187–1200. [PubMed: 28622506]

Santos D, Luzio A, and Coimbra AM (2017). Zebrafish sex differentiation and gonad development: A review on the impact of environmental factors. Aquat. Toxicol 191, 141–163. [PubMed: 28841494]

Schneider CA, Rasband WS, and Eliceiri KW (2012). NIH Image to ImageJ: 25 years of image analysis. Nat. Methods 9, 671–675. [PubMed: 22930834]

Semotok JL, Cooperstock RL, Pinder BD, Vari HK, Lipshitz HD, and Smibert CA (2005). Smaug recruits the CCR4/POP2/NOT deadenylase complex to trigger maternal transcript localization in the early Drosophila embryo. Curr. Biol 15, 284–294. [PubMed: 15723788]

Shi H, Wang X, Lu Z, Zhao BS, Ma H, Hsu PJ, Liu C, and He C. (2017). YTHDF3 facilitates translation and decay of N6-methyladenosine-modified RNA. Cell Res. 27, 315–328. [PubMed: 28106072]

Shi H, Wei J, and He C. (2019). Where, When, and How: Context-Dependent Functions of RNA Methylation Writers, Readers, and Erasers. Mol. Cell 74, 640–650. [PubMed: 31100245]

Subtelny AO, Eichhorn SW, Chen GR, Sive H, and Bartel DP (2014). Poly(A)-tail profiling reveals an embryonic switch in translational control. Nature 508, 66–71. [PubMed: 24476825]

Tadros W, and Lipshitz HD (2009). The maternal-to-zygotic transition: a play in two acts. Development 136, 3033–3042. [PubMed: 19700615]

Tadros W, Goldman AL, Babak T, Menzies F, Vardy L, Orr-Weaver T, Hughes TR, Westwood JT, Smibert CA, and Lipshitz HD (2007). SMAUG is a major regulator of maternal mRNA destabilization in Drosophila and its translation is activated by the PAN GU kinase. Dev. Cell 12, 143–155. [PubMed: 17199047]

Temme C, Zhang L, Kremmer E, Ihling C, Chartier A, Sinz A, Simonelig M, and Wahle E. (2010). Subunits of the Drosophila CCR4-NOT complex and their roles in mRNA deadenylation. RNA 16, 1356–1370. [PubMed: 20504953]

Thisse B, and Thisse C. (2014). In situ hybridization on whole-mount zebrafish embryos and young larvae. Methods Mol. Biol 1211, 53–67.

Ulitsky I, Shkumatava A, Jan CH, Subtelny AO, Koppstein D, Bell GW, Sive H, and Bartel DP (2012). Extensive alternative polyadenylation during zebrafish development. Genome Res. 22, 2054–2066. [PubMed: 22722342]

Vastenhouw NL, Cao WX, and Lipshitz HD (2019). The maternal-to-zygotic transition revisited. Development 146, 146.

Vejnar CE, and Giraldez AJ (2020). LabxDB: versatile databases for genomic sequencing and lab management. Bioinformatics 36, 4530–4531. [PubMed: 32502232]

Vejnar CE, Moreno-Mateos MA, Cifuentes D, Bazzini AA, and Giraldez AJ (2016). Optimized CRISPR-Cas9 system for genome editing in zebrafish. Cold Spring Harb. Protoc 2016, 856–870.

Vejnar CE, Abdel Messih M, Takacs CM, Yartseva V, Oikonomou P, Christiano R, Stoeckius M, Lau S, Lee MT, Beaudoin JD, et al. (2019). Genome wide analysis of 3¿ UTR sequence elements and proteins regulating mRNA stability during maternal-to-zygotic transition in zebrafish. Genome Res. 29, 1100–1114. [PubMed: 31227602]

Voeltz GK, and Steitz JA (1998). AUUUA sequences direct mRNA deadenylation uncoupled from decay during Xenopus early development. Mol. Cell. Biol 18, 7537–7545. [PubMed: 9819439]

Wagner DS, Dosch R, Mintzer KA, Wiemelt AP, and Mullins MC (2004). Maternal control of development at the midblastula transition and beyond: mutants from the zebrafish II. Dev. Cell 6, 781–790. [PubMed: 15177027]

Wang X, Lu Z, Gomez A, Hon GC, Yue Y, Han D, Fu Y, Parisien M, Dai Q, Jia G, et al. (2014). N6-methyladenosine-dependent regulation of messenger RNA stability. Nature 505, 117–120. [PubMed: 24284625]

Wang X, Zhao BS, Roundtree IA, Lu Z, Han D, Ma H, Weng X, Chen K, Shi H, and He C. (2015). N6-methyladenosine modulates messenger RNA translation efficiency. Cell 161, 1388–1399. [PubMed: 26046440]

Weidmann CA, Raynard NA, Blewett NH, Van Etten J, and Goldstrohm AC (2014). The RNA binding domain of Pumilio antagonizes poly-adenosine binding protein and accelerates deadenylation. RNA 20, 1298–1319. [PubMed: 24942623]

Wojtas MN, Pandey RR, Mendel M, Homolka D, Sachidanandam R, and Pillai RS (2017). Regulation of m6A Transcripts by the 3′®5′ RNA Helicase YTHDC2 Is Essential for a Successful Meiotic Program in the Mammalian Germline. Mol. Cell 68, 374–387.e12. [PubMed: 29033321]

Wu Q, Medina SG, Kushawah G, DeVore ML, Castellano LA, Hand JM, Wright M, and Bazzini AA (2019). Translation affects mRNA stability in a codon-dependent manner in human cells. eLife 8, 8.

Yartseva V, and Giraldez AJ (2015). The Maternal-to-Zygotic Transition During Vertebrate Development: A Model for Reprogramming. In Current Topics in Developmental Biology (Academic Press Inc.), pp. 191–232.

Zaccara S, and Jaffrey SR (2020). A Unified Model for the Function of YTHDF Proteins in Regulating m6A-Modified mRNA. Cell 181, 1582–1595.e18. [PubMed: 32492408]

Zaccara S, Ries RJ, and Jaffrey SR (2019). Reading, writing and erasing mRNA methylation. Nat. Rev. Mol. Cell Biol 20, 608–624. [PubMed: 31520073]

Zhao BS, Wang X, Beadell AV, Lu Z, Shi H, Kuuspalu A, Ho RK, and He C. (2017). m6A-dependent maternal mRNA clearance facilitates zebrafish maternal-to-zygotic transition. Nature 542, 475–478. [PubMed: 28192787]

Highlights

- M^6A methylation promotes maternal mRNA deadenylation
- Individual Ythdf readers are not obligatory for maternal mRNA clearance
- Ythdf readers function redundantly in ovary development and zebrafish viability
- miR-430 acts additively with m^6A to promote enhanced maternal mRNA degradation

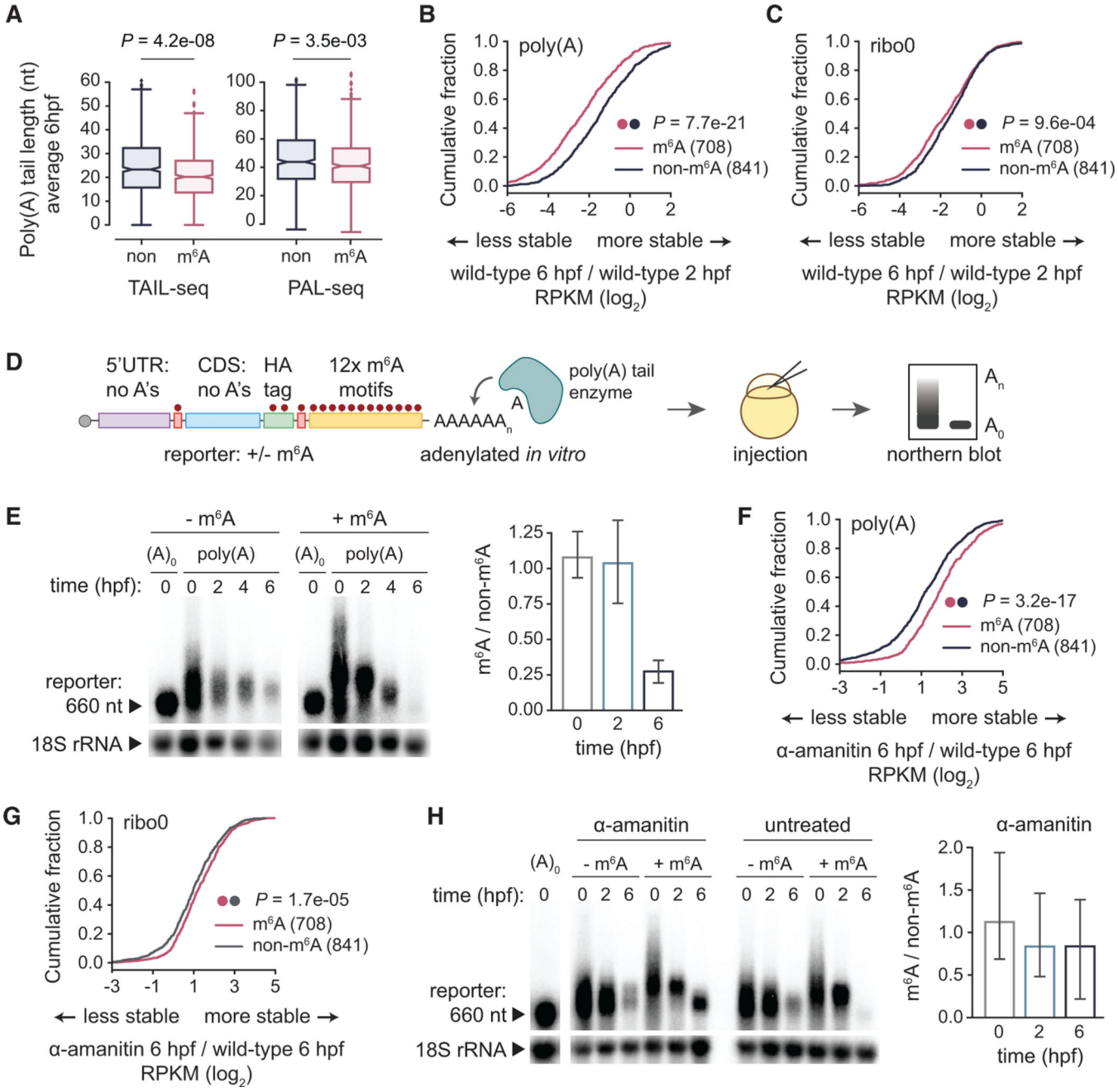

Figure 1. m^{6}A Methylation Promotes Deadenylation of Maternal mRNAs

(A) Average poly(A) tail lengths at 6 hpf for m^{6}A-modified (m^{6}A, n = 675) and non-modified (non, n = 841) maternal mRNAs from TAIL-seq and PAL-seq datasets. Box, first to last quartiles; whiskers, 1.5× interquartile range; center line, median; diamonds, outliers.

(B and C) Cumulative distributions of fold changes in maternal mRNA abundance ($\log_2$ RPKM) between 6 and 2 hpf in wild-type embryos, for m^{6}A-modified (n = 708) and non-modified mRNAs (n = 841), from poly(A) (B) or ribo0 (C) mRNA-seq.

(D) Schematic of methylated mRNA reporter assay. The mRNA reporter had a 5′ UTR and CDS without adenines, AUG start, and UAG stop codons, and 3′ UTR with 12× m^{6}A motifs

(GGACT). The reporter was *in vitro* transcribed with or without m^6A-modified adenines and polyadenylated. Reporter mRNA was injected into embryos and mRNA levels and polyadenylation were visualized by Northern blots.

(E) Northern blot of m^6A-modified (+m^6A) and unmodified (−m^6A) reporter at various time points (hpf) in wild-type embryos. Loading control (18S rRNA, ~1,900 nt) on bottom. Ratio of m^6A to non-m^6A reporter abundance (18S rRNA normalized, mean ± SD, n = 5 independent replicates) on right. A_0, reporter injected without poly(A) tail.

(F and G) Cumulative distributions of fold changes in maternal mRNA abundance (log_2 RPKM) between α-amanitin treated and wild-type at 6 hpf, for m^6A-modified (n = 708) and non-modified mRNAs (n = 841), from poly(A) (F) or ribo0 (G) mRNA-seq.

(H) Northern blot of m^6A-modified (+m^6A) and unmodified (−m^6A) reporter at various time points (hpf) in α-amanitin and untreated embryos. Loading control (18S rRNA, ~1,900 nt) on bottom. Ratio of m^6A to non-m^6A reporter abundance (18S rRNA normalized, mean ± SD, n = 3 independent replicates) for α-amanitin on right. A_0, reporter injected without poly(A) tail.

p values (A–C, F–G) were computed by a Mann-Whitney U test.

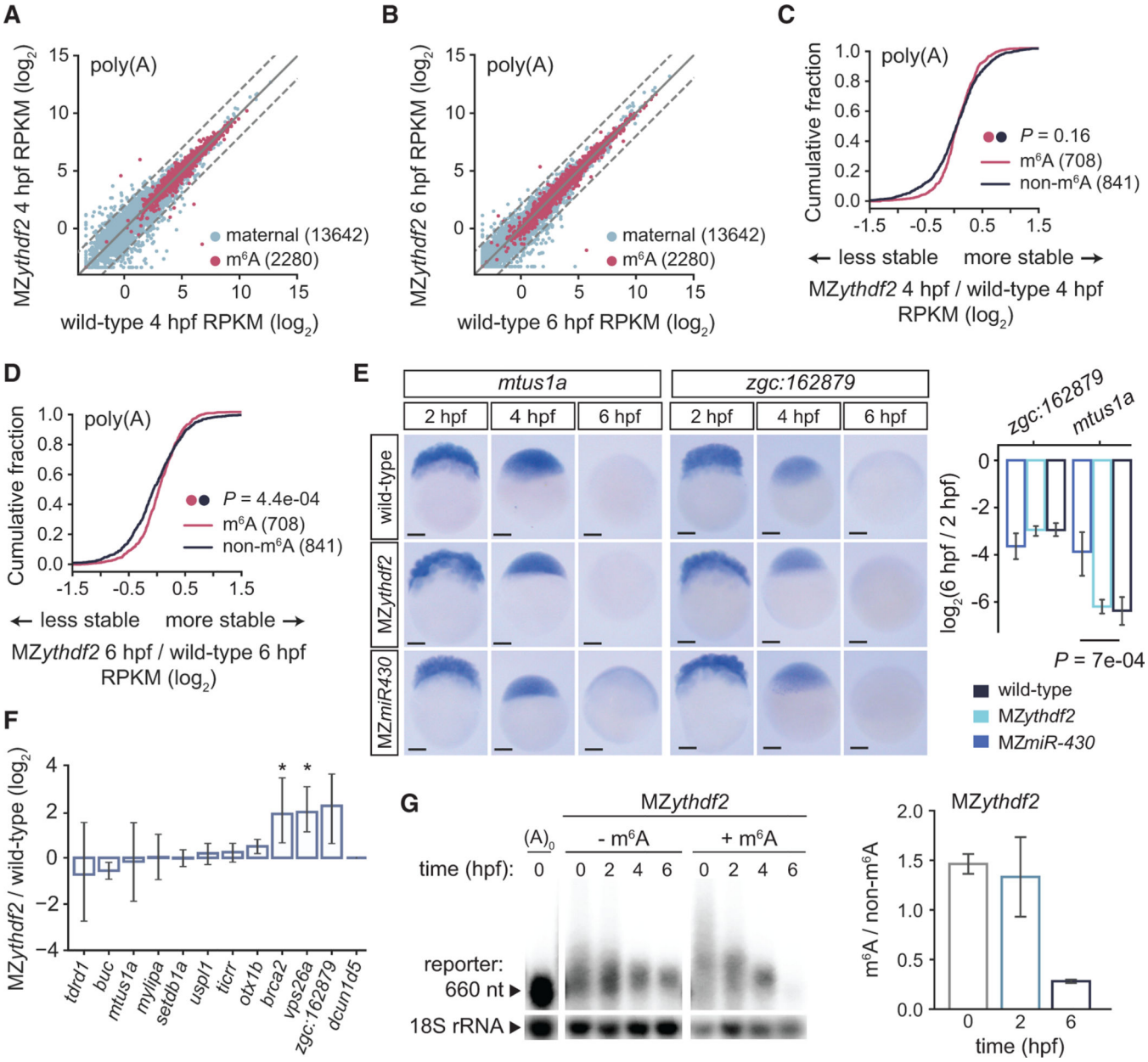

Figure 2. Ythdf2 Is Not Mandatory for Global Maternal Clearance but Marginally Contributes to m^{6}A-Mediated Decay

(A and B) Biplots of expression ($\log_2$ RPKM) of maternal (n = 13,642) and m^{6}A-modified mRNAs (n = 2,280) between wild-type and MZ*ythdf2* at 4 (A) or 6 (B) hpf, from poly(A) mRNA-seq. Dashed lines, 2-fold change.

(C and D) Cumulative distributions of fold changes in maternal mRNA abundance ($\log_2$ RPKM) between MZ*ythdf2* and wild-type at either 4 (C) or 6 (D) hpf, for m^{6}A-modified (n = 708) and non-modified mRNAs (n = 841), from poly(A) mRNA-seq. p values computed by a Mann-Whitney U test.

(E) *In situs* of methylated maternal mRNAs *mtus1a* and *zgc:162879* in wild-type, MZ*ythdf2*, and MZ*mir-430* embryos at 2, 4, or 6 hpf. qRT-PCR mRNA abundance fold change ($\log_2$,

6 versus 2 hpf, mean ± SD, n = 3 independent replicates) on right. p values computed by a two-sided Student's t test. Scale bars, 100 μM.

(F) Methylated maternal mRNA abundance fold changes from qRT-PCR at 4 hpf between MZ*ythdf2* and wild-type (mean ± SD, n = 3 independent replicates). Only *brca2* (p = 5.4e−03) and *vps26a* (p = 6.3e−03) were significantly stabilized.

(G) Northern blot of m^6A-modified (+m^6A) versus unmodified (−m^6A) reporter at various time points (hpf) in MZ*ythdf2* embryos. Loading control (18S rRNA, ~1,900 nt) on bottom. Ratio of m^6A to non-m^6A reporter abundance (18S rRNA normalized, mean ± SD, n = 2 independent replicates) on right. A_0, reporter injected without poly(A) tail.

For (A) –(F), wild-type label represents background-matched wild-type controls.

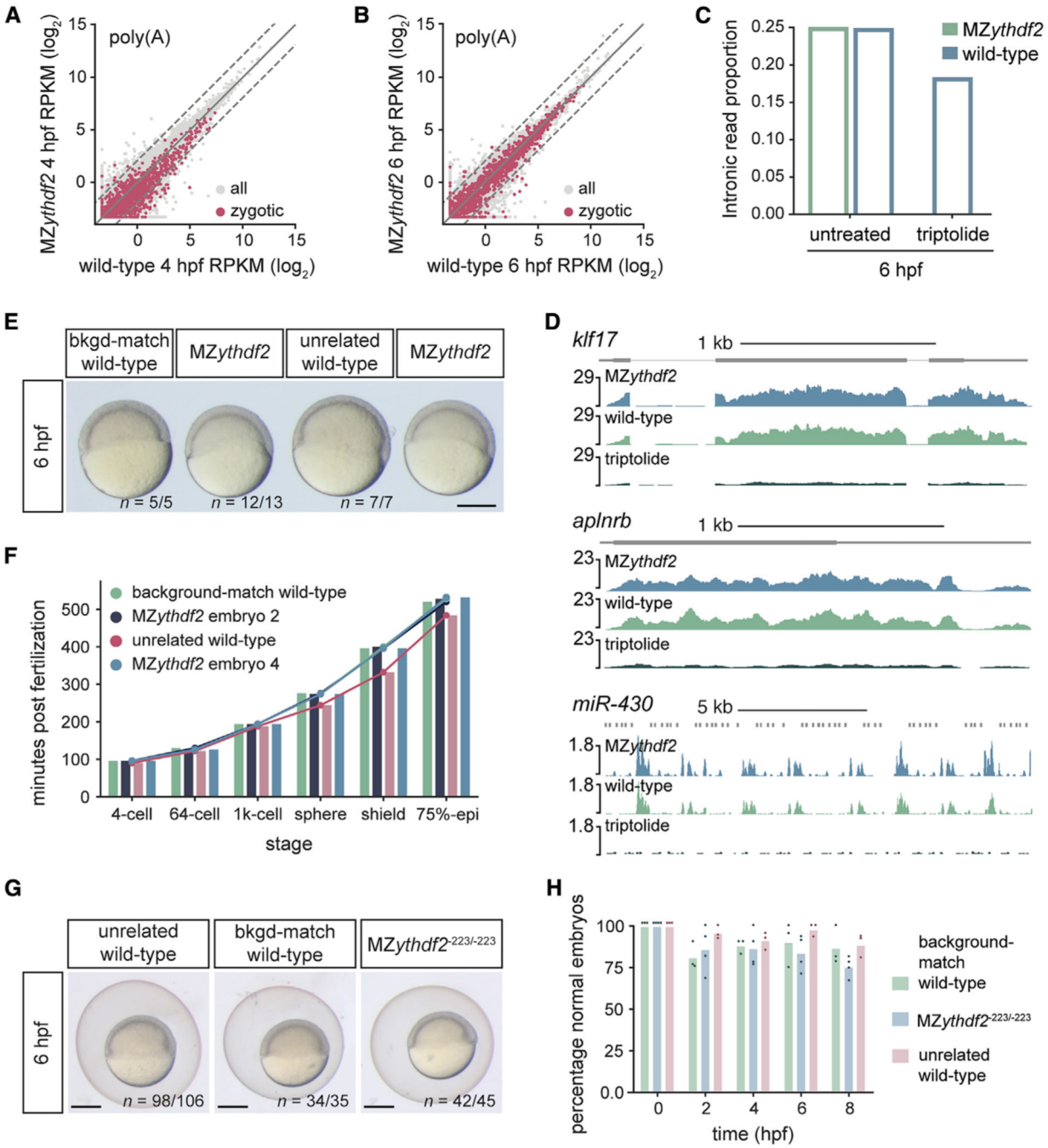

Figure 3. Loss of Ythdf2 Does Not Hinder Zygotic Genome Activation or Onset of Gastrulation

(A and B) Biplots of expression of zygotic (n = 1,760) and all mRNAs (n = 20,119) between wild-type and MZ*ythdf2* embryos at 4 (A) or 6 (B) hpf, from poly(A) Mrna-seq. Dashed lines, 2-fold change.

(C) Proportion of intronic reads relative to total read number for wild-type, MZ*ythdf2*, and triptolide-treated embryos at 6 hpf from ribo0 mRNA-seq.

(D) Genome tracks of zygotic transcripts in MZ*ythdf2*, wild-type, and triptolide-treated embryos from 6 hpf poly(A) mRNA-seq. Fold-changes (log_2 RPKM) for *aplnrb*, *klf17*, and

miR-430 were 0.04, −0.21, and −0.32, respectively, for MZ*ythdf2* versus wild-type, and −2.67, −3.08, and −3.83, respectively, for triptolide versus wild-type.

For (A)–(D), wild-type controls were background-matched wild-type embryos.

(E) Image of zebrafish embryos where MZ*ythdf2* and background-matched (bkgd-match) wild-type (see Figure S2A) exhibit similar developmental delay relative to unrelated wild-type at 6 hpf. Image is from time-lapse movie (Video S1). MZ*ythdf2* embryos are from the same clutch. n, replicate number of embryos at same developmental stage. Scale bar, 500 μM.

(F) Quantification of developmental rates of embryos in (E, Video S1). Bars and dots indicate minutes post fertilization at which embryos reach corresponding developmental stage. MZ*ythdf2* embryos 2 and 4 correspond to the embryos second from left and on far right in (E), respectively.

(G) Representative images of MZ*ythdf2*$^{-223/-223}$, background-matched (bkgd-match) wild-type, and unrelated wild-type embryos at 6 hpf. n, replicate number of embryos at same developmental stage. Scale bars, 500 μM.

(H) Quantification of normally developing embryos is similar for each genotype. Dots indicate quantifications from three independent clutches and bars show mean percentage of normally developed embryos at each time point (hpf) from all clutches.

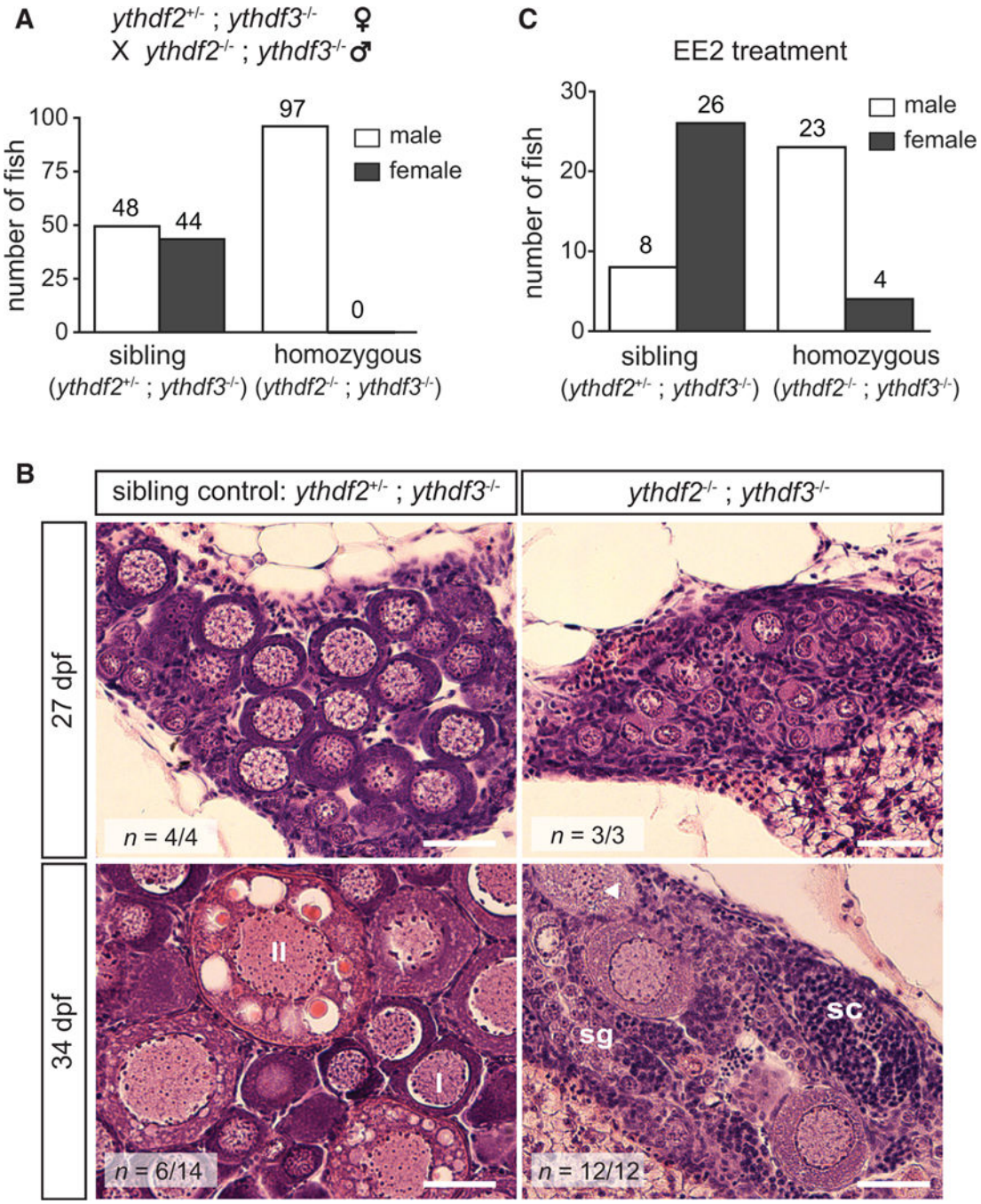

Figure 4. Ythdf2 and Ythdf3 Are Redundantly Required for Zebrafish Ovary Development

(A) Numbers of male and female fish of each genotype. Sibling control and double *ythdf2;ythdf3* homozygotes were offspring from the same cross, depicted on top.

(B) Gonad histology of double homozygous (*ythdf2*$^{-/-}$;*ythdf3*$^{-/-}$) and sibling control fish from the cross in (A). At 27 dpf, mutants exhibit less developed juvenile ovaries than controls. At 35 dpf, 6 sibling fish had adult ovaries and 8 had testes, while all 12 *ythdf2*$^{-/-}$;*ythdf3*$^{-/-}$fish had testes. I, stage I oocytes; II, stage II oocytes; triangle, apoptotic oocyte;

sg, spermatogonia; sc, spermatocytes. n, replicate number with similar gonads. Scale bars, 40 μm.

(C) Numbers of male and female fish of each genotype, following treatment with 17α-ethynylestradiol (EE2). Fish were from the same cross as in (A).

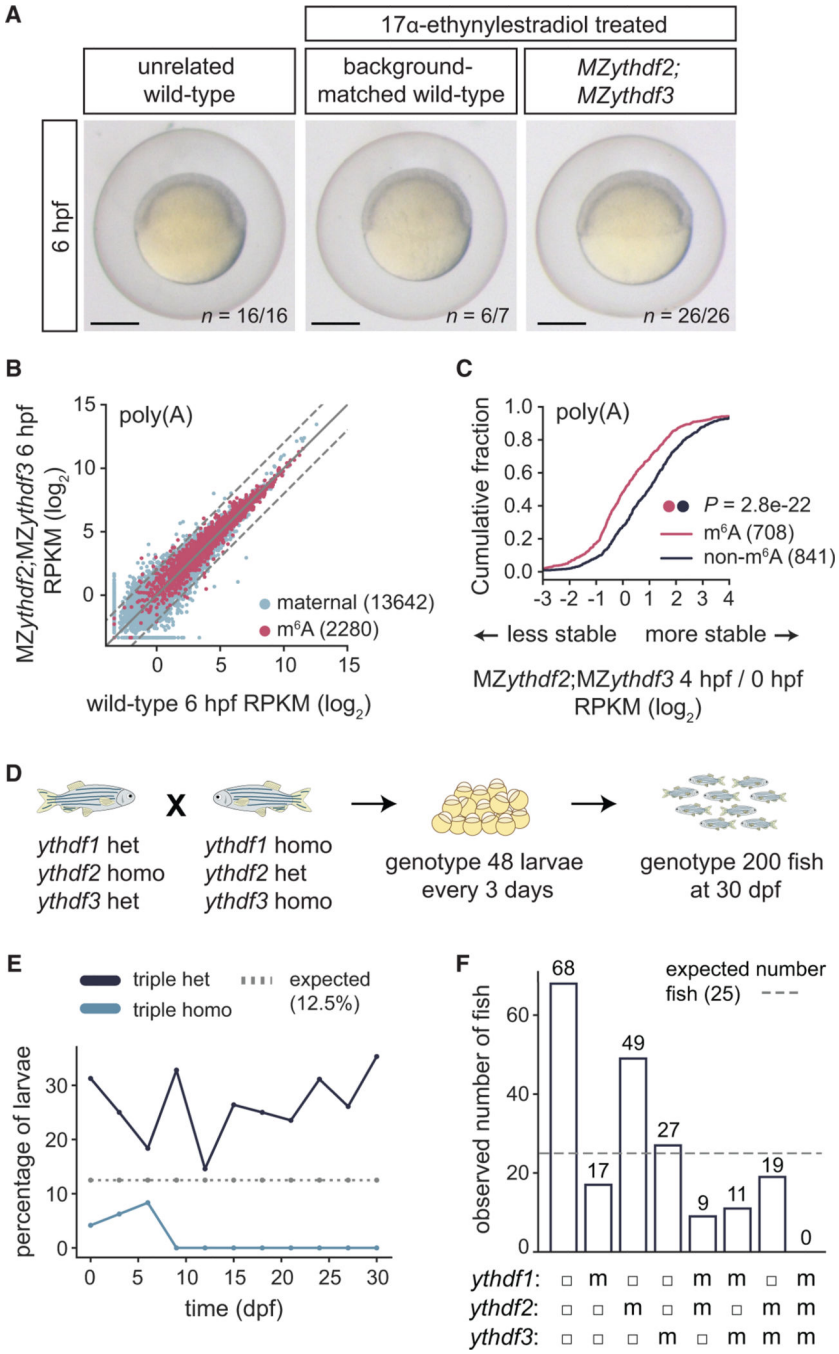

Figure 5. Triple Loss of Ythdf Readers Disrupts Zebrafish Development

(A) MZ*ythdf2*;MZ*ythdf3*, background-matched wild-type, and unrelated TU-AB wild-type zebrafish embryos develop at similar rates. Parents of mutant and background-matched control embryos were 17α-ethynylestradiol treated. n, replicate number of embryos at same developmental stage. Scale bars, 500 μm.

(B) Biplot of expression (log_2 RPKM) of maternal (n = 13,642) and m^6A-modified (n = 2,280) mRNAs between wild-type and MZ*ythdf2*;MZ*ythdf3*, from 6 hpf poly(A) mRNA-seq. Dashed lines, 2-fold change.

(C) Cumulative distribution of fold changes in maternal mRNA abundance (log_2 RPKM) between 4 and 0 hpf in MZ*ythdf2*;MZ*ythdf3* embryos, for m^6A-modified (n = 708) and non-modified (n = 841) mRNAs, from poly(A) mRNA-seq. p values computed by a Mann-Whitney U test.

(D) Schematic of cross and genotyping strategy for triple Ythdf mutants. Female fish (*ythdf1*$^{+/-}$;*ythdf2*$^{-/-}$;*ythdf3*$^{+/-}$) were crossed to males (*ythdf1*$^{-/-}$;*ythdf*$^{+/-}$;*ythdf3*$^{-/-}$) to generate triple homozygotes (1 of 8 possible genotypes). Every 3 days, 48 larvae were genotyped, with 200 more fish genotyped at 30 dpf.

(E) Percentage of triple heterozygous (het) or triple homozygous (homo) fish during development. Dotted line, expected percentage (12.5%) of each genotype, from cross in (D).

(F) Number of fish with each genotype from cross in (D) at 30 dpf. For each *ythdf* allele: filled circle, heterozygous; m, homozygous. Dotted line, expected fish number (25), equal for all genotypes.

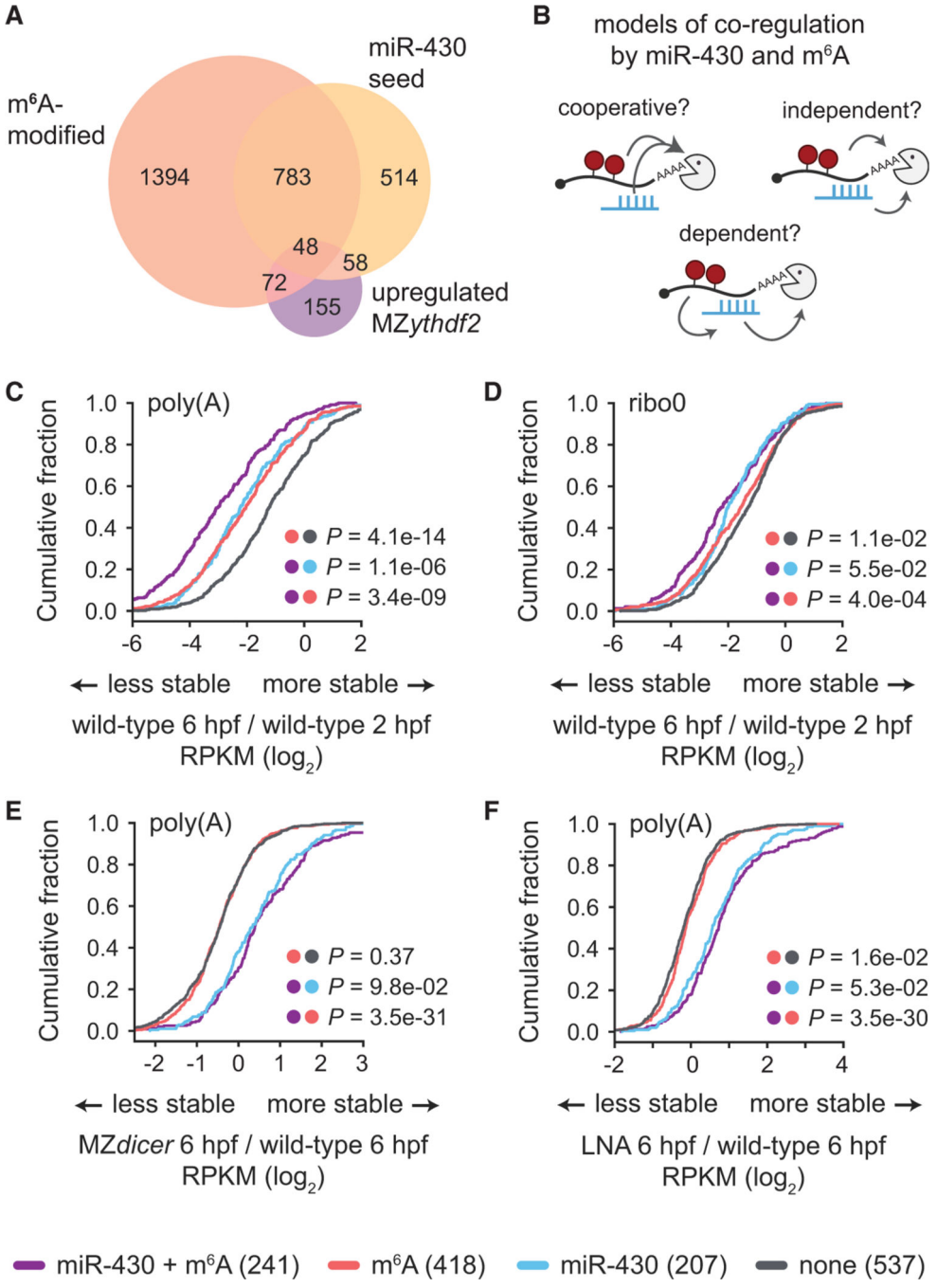

Figure 6. miR-430 and m^{6}A Pathways Are Independent and Co-regulate Maternal mRNAs for Destabilization

(A) Venn diagram of numbers of maternal mRNAs with a miR-430 seed in the 3′ UTR, are m^{6}A modified, are stabilized in MZ*ythdf2* (fold change > 0.5), or have overlapping features. (B) Schematic of potential mechanisms of miR-430 and m^{6}A co-regulation, tested in (C)–(F). The pathways could function cooperatively, enhancing decay of common targets, independently, acting additively on common targets, or m^{6}A could be dependent on miR-430, causing disruption of m^{6}A-based mRNA decay upon loss of miR-430.

(C–F) Cumulative distributions of fold changes in maternal mRNA abundance ($\log_2$ RPKM) for transcripts that are targets of both m^6A and miR-430 (miR-430 + m^6A, n = 241), m^6A only (m^6A, n = 418), miR-430 only (miR-430, n = 207), or neither (none, n = 537) from poly(A) (C, E, F) or ribo0 (D) mRNA-seq. Fold-change comparisons were between 6 and 2 hpf in wild-type (C, D) or at 6 hpf between MZ*dicer* (E) or LNA-treated (F) embryos and wild-type controls. Dots indicate groups compared for corresponding p values, computed by a Mann-Whitney U test. Legend on bottom.

KEY RESOURCES TABLE

REAGENT or RESOURCE	SOURCE	IDENTIFIER
Antibodies		
rabbit anti-Ythdf1	this manuscript	Ynzyme custom order
rabbit anti-Ythdf2	this manuscript	Ynzyme custom order
rabbit anti-Ythdf3	this manuscript	Ynzyme custom order
rabbit anti-Actin	Abcam	Cat# ab8227; RRID: AB_2305186
goat anti-rabbit IgG, (H+L) HRP conjugate	Millipore	Cat# AP307P; RRID: AB_92641
Chemicals, Peptides, and Recombinant Proteins		
triptolide	Sigma-aldrich	Cat# T3652
α-amanitin	Sigma-aldrich	Cat# A2263
low melt agarose	AmericanBio	Cat# CAS: 9012-36-6
N^6-methyladenosine 5'-triphosphate	TriLink	Cat# N-1013–5
$m^7G(5')ppp(5')G$ RNA cap structure analog	New England BioLabs	Cat# S1404S
17 α-ethynylestradiol (EE2)	Sigma-Aldrich	Cat# E4876
Critical Commercial Assays		
AmpliScribe-T7-Flash Transcription kit	Epicenter	Cat# ASF3257
HiScribe SP6 RNA Synthesis Kit	New England BioLabs	Cat# E2070S
mMessage mMachine SP6 Transcription Kit	Invitrogen	Cat# 74104
Nick Translation Kit	Sigma-Aldrich	Cat# 10976776001
Poly(A) tailing kit	Invitrogen	Cat# AM1350
Power SYBR Green PCR Master Mix	Applied Biosystems	Cat# 4368706
Protein A Dynabeads	Invitrogen	Cat# 10008D
RNeasy RNA extraction kit	QIAGEN	Cat# AM1340
Superscript III Reverse Transcriptase kit	Invitrogen	Cat# 18080093
TRIzol reagent	Invitrogen	Cat# 15596–018
Deposited Data		

REAGENT or RESOURCE	SOURCE	IDENTIFIER
mRNA-sequencing of MZ*ythdf2*, MZ*ythdf2*;MZ*ythdf3*, or MZ*dicer* mutants	this manuscript	SRP297464
mRNA-sequencing of MZ*ythdf2* mutants	Zhao et al., 2017	GSE79213
mRNA-sequencing time course of zebrafish embryos	Vejnar et al., 2019 Beaudoin et al., 2018 Bazzini et al., 2016	SRP189512 SRP149556 SRP072296
PAL-sequencing in zebrafish embryos	Subtelny et al., 2014	GSE52809
TAIL-sequencing in zebrafish embryos	Chang et al., 2018	https://doi.org/10.5281/zenodo.2640028
Experimental Models: Organisms/Strains		
Zebrafish: TU-AB and TLF strains	Zebrafish International Resource Center	N/A
Zebrafish: *miR-430* cluster deletion mutant	Liu et al., 2013	N/A
Zebrafish: *ythdf2* −8bp mutants	Zhao et al., 2017	N/A
Zebrafish*: dicer* mutants	Giraldez et al., 2006	N/A
Zebrafish*: mettl3* mutants	this manuscript	N/A
Zebrafish: *mettl14* mutants	this manuscript	N/A
Zebrafish: *ythdf1* mutants	this manuscript	N/A
Zebrafish: *ythdf2* −223bp mutants	this manuscript	N/A
Zebrafish: *ythdf3* mutants	this manuscript	N/A
Zebrafish: *ythdf2*;*ythdf3* double mutants	this manuscript	N/A
Zebrafish: *ythdf1*;*ythdf2*;*ythdf3* triple mutants	this manuscript	N/A
Oligonucleotides		
See Table S3 for primers and oligonucleotides used in this manuscript		
Recombinant DNA		
pSP64T-ythdf1-3xflag	this manuscript	Addgene #164488
pSP64T-ythdf2-3xflag	this manuscript	Addgene #164489
pSP64T-ythdf3-3xflag	this manuscript	Addgene #164490
pCS2+methylated-reporter	this manuscript	Addgene #164491
pT3TS-nCas9n	Jao et al., 2013	Addgene #46757
Software and Algorithms		

Cell Rep. Author manuscript; available in PMC 2024 September 17.

REAGENT or RESOURCE	SOURCE	IDENTIFIER
STAR	Dobin et al., 2013	https://github.com/alexdobin/STAR
Python (data analysis)	Python 3.8	https://www.python.org
DESeq2	Love et al., 2014	https://bioc.ism.ac.jp/packages/3.1/bioc/html/DESeq2.html
ImageJ	Schneider et al., 2012	https://imagej.nih.gov/ij/
SnapGene	GSL Biotech	snapgene.com
CRISPRscan	Moreno-Mateos et al., 2015	crisprscan.org